Journal of the Korean Ceramic Society (2024) 61:367–390
https://doi.org/10.1007/s43207-024-00365-1

REVIEW

A review of photocatalytic CO_2 reduction: exploring sustainable carbon emission mitigation from thermodynamics to kinetics and strategies for enhanced efficiency

Hassan Akbar[1,3] · Muhammad Subhan Javed[2] · Syeda Tehreem Iqbal[2] · Muhammad Iftikhar Khan[2] · Tauseef Anwar[6] · Faiza Anjum[2] · Ashfaq Ahmad[4] · Muhammad Muneeb[2] · Asghar Ali[2] · Won-Chun Oh[5]

Received: 29 October 2023 / Revised: 11 December 2023 / Accepted: 5 January 2024 / Published online: 21 February 2024

Abstract

To mitigate the increased CO_2 emission, CO_2 reduction to multi-carbon fuels or other useable substances is an appealing yet essential approach. Since, reduction of CO_2 is a thermodynamically uphill process, an economical CO_2 fixation is only achievable if energy source used is of renewable energy such as solar energy. Photocatalytic CO_2 reduction is a complex process due to its dependency on catalyst design, selectivity, efficiency, and photostability. The competence of a photocatalytic CO_2 reduction reaction is effected by factors, such as the type of photocatalyst used their band-gap energy, surface area, and structure of the crystal. This review discusses the kinetics and thermodynamics of photocatalytic CO_2 reduction and considers the effects of parameters like defects and impurity doping on photocatalysis. The study also focusses on the selectivity of products, i.e., methane, methanol, formaldehyde, etc. This comprehensive review provides insights into the development and improvement of photocatalytic efficiency for CO_2 photoreduction, contributing to the reduction of carbon emissions and a more sustainable future.

Keywords Photocatalytic CO_2 reduction · CO_2 to fuels · Impurity doping · Kinetic model · Structural defects

1 Introduction

Human activities, particularly the combustion of fossil fuels, such as coal, oil, and natural gas, have markedly increased CO_2 emissions. This surplus of CO_2 intensifies the greenhouse effect, trapping heat within Earth's atmosphere, consequently leading to global warming and alterations in climate patterns. The mitigation of CO_2 emissions stands as a pivotal aspect in addressing climate change and safeguarding the environment [1]. The stability of carbon dioxide arises from its molecular structure and the thermodynamics governing the chemical processes involved—specifically, the carbon–oxygen bonds in CO_2 exhibit notable strength. The formation of this compound releases a substantial amount of energy [2]. To curtail CO_2 emissions, diverse effective strategies exist. These encompass measures, such as transitioning to sustainable energy sources, advocating for energy conservation, adopting cleaner transportation methods, refining waste management practices, and supporting reforestation initiatives. One prevalent method employed for CO_2 reduction is carbon capture and storage (CCS), which involves capturing CO_2 emissions

Hassan Akbar and Muhammad Subhan Javed have contributed equally to this work.

✉ Asghar Ali
asghar246@gmail.com

✉ Won-Chun Oh
wc_oh@hanseo.ac.kr

1 Department of Physics, Abbottabad University of Science and Technology (AUST), Abbottabad, Pakistan

2 Department of Physics, The University of Lahore, 1-km, Defense Road, Lahore, Pakistan

3 College of Environmental Science and Engineering, North China Electric Power, University 2 Beinong Road, Changing District, Beijing 102206, China

4 School of Material Science and Engineering, Shanghai Jiaotong University, Shanghai, China

5 Department of Advanced Materials Science and Engineering, Hanseo University, 46, Hanseo Ro, Haemi-myun, Seosan, Chungnam, Republic of Korea

6 Department of Physics, Division of Science and Technology, University of Education Lahore, Lahore 54770, Pakistan

from industrial processes or power generation facilities and subsequently securely storing them underground. Another notable approach is carbon utilization or recycling, wherein captured CO_2 is converted into valuable products such as fuels, chemicals, and construction materials. Furthermore, some researchers are engaged in developing innovative catalysts and processes for the direct conversion of CO_2 into useful chemicals and fuels through electrochemical or chemical reactions [3]. These endeavors are geared toward converting CO_2 from a greenhouse gas into valuable resources, thereby contributing to the reduction of CO_2 emissions and fostering a more sustainable future. Robust research and development in this domain are imperative for combatting climate change and achieving practical carbon management. Another encouraging process known as artificial photocatalytic system (APS), involves photocatalysts, typically semiconductor materials, to harness solar energy for the conversion of CO_2 into valuable products [4]. Catalytic environmental remediation holds paramount importance owning to its potential to expedite chemical reactions crucial to pollutant degradation without being consumed in process. Catalysts act by increasing reaction rates, lowering activation energy and fostering selectivity and specificity toward target contamination. This technology is promising avenue for mitigating CO_2 emission and has the potential to play a crucial role in the transition toward a low carbon future. Photocatalysts can be used for the separation of water molecule into H_2 and O_2 utilizing solar energy for this purpose [5–8]. Photoreduction of CO_2 is of great interest. It is studied globally to overcome the world's energy crises [9, 10]. Researcher are dedicated to develop effective photocatalyst for the conversion of H_2O to molecules and reduction of CO_2 into fuels (H_2, CH_3OH, CH_4, CO, HCHO, and HCOOH) [11]. Photocatalytic CO_2 reduction is more complex due to reasons like selectivity, efficiency, catalyst design, energy requirements, and photostability [12–14]. Due to these reasons, an artificial need for photosynthesis is required which aims to improve the conversion of CO_2 and water. The primary objective behind the development of efficient photocatalyst for water splitting and CO_2 reduction is to harness the abundant and sustainable power of sunlight as a driving force for chemical reaction. This endeavor addresses two critical global challenges: the transition to clean energy sources and reduction of carbon emission. Catalysts that are explored so far are either homogenous or heterogeneous catalysts. Heterogeneous catalysts are in different phase from the reactants, making it easier to separate them from reaction mixture by catalysts' recycling. This reduces the chances of contamination and provides larger surface area for reactants to interact [5, 15–17]. Various semiconductors are used for photoreduction of CO_2 like TiO_2 [18–20], $BiVO_4$ [21–23], MOFs [24–26], metal halide perovskite [27–29], etc. The photoreduction is basically a surface/interface reaction [30]. The key requirements are needed to be met to effectively utilize the energy from visible-light spectrum for photocatalytic reaction, which include appropriate band gap [31], photogenerated charge separation [32, 33], selectivity, stability, and activity for existing photocatalytic CO_2 photoreduction. Facilitating the efficient generation of charge carriers through light absorption and subsequent surface reactions are essential aspects of CO_2 photoreduction as they determine the whole efficiency and selectivity of the process in converting CO_2 into valuable fuels or chemicals [4, 34, 35]. Previous research has shown that defects in photocatalytic materials can alter their electronic structure and optical properties [36–39]. These defects could be minimized by doping, enabling the material to absorb a wider range of light and promoting efficient charge separation and reducing recombination rates [40–42]. There is an increasing interest in harnessing CO_2, the most abundant and economically viable carbon-rich resource, for the progress of alternating energy innovation [43]. The concept of utilizing photocatalytic reactions for sustainable solar energy, to transform atmospheric CO_2 waste into alternative fuels, offers a feasible resolution. This innovation strategy not only diminishes carbon dioxide emissions but also concurrently upcycle it as a renewable fuel increasing solar energy resources [44]. Effective photocatalytic performance hinges on various factors, in which the presence of highly efficient photocatalyst stands out as a pivotal determinant. Conversely, optimizing light absorption, minimizing photon losses, and mitigating charge carrier recombination have garnered considerable focus in shaping a more proficient designing of catalyst. The main goal of this review paper is to furnish an extensive literature overview concerning the evolution of various catalysts for conversion of CO_2 to other fuels. In this context, the paper provides a thorough examination of the working mechanism, developmental aspects, and proactive measure aimed at addressing CO_2 photocatalytic reduction. Additionally, it offers insight into future objectives and directions. The overarching aim of this review is to furnish essential background knowledge and outline general research pathways for individuals engaged or intending to enter the domain of CO_2 conversion processes.

2 Thermodynamics of photocatalytic CO_2 reduction

Thermodynamics of CO_2 reduction reaction is found to be contingent on redox potential ΔE° and Gibbs free energy ΔG° [45]. Due to highly positive ΔG°, which indicates that the reaction is endothermic and not favorable under standard conditions, CO_2 reduction is an energetically uphill and non-spontaneous process [46, 47], which means that it requires an input of energy to proceed and it is not favorable for normal temperature and pressure ranges. Compared to water splitting where ΔG° is negative, indicating thermodynamic favorability and spontaneity under standard conditions, CO_2

reduction requires significantly more energy to drive the process. Therefore, the energy storage ratio of CO_2 reduction, i.e., the amount of energy needed for the reaction compared to the energy stored in the resulting products, is generally much higher than that for water splitting [48–50]. The reactions along with the redox potential and Gibbs free energy are given below from Eqs. 1–6 in which Eq. 1 shows the water splitting, while Eqs. 2–6 shows CO_2 reduction [51]

$$H_2O_{(l)} \rightarrow H_{2(g)} + 1/2O_{2(g)},$$
$$\Delta G^\circ = 237\,\text{kj/mol}, \quad \Delta E^\circ = 1.23\,\text{V} \tag{1}$$

$$CO_{2(g)} \rightarrow CO_{(g)} + 1/2O_{2(g)},$$
$$\Delta G^\circ = 257\,\text{kj/mol}, \quad \Delta E^\circ = 1.33\,\text{V} \tag{2}$$

$$CO_{2(g)} + H_2O_{(l)} \rightarrow HCOOH_{(l)+1/2}O_{2(g)},$$
$$\Delta G^\circ = 286\,\text{kj/mol}, \quad \Delta E^\circ = 1.48\,\text{V} \tag{3}$$

$$CO_{2(g)} + H_2O_{(l)} \rightarrow HCHO_{(l)} + O_{2(g)},$$
$$\Delta G^\circ = 522\,\text{kj/mol}, \quad \Delta G^\circ = 1.35\,\text{V} \tag{4}$$

$$CO_{2(g)} + 2H_2O_{(l)} \rightarrow CH_3OH_{(l)} + 3/2O_{2(g)},$$
$$\Delta G^\circ = 703\,\text{kj/mol}, \quad \Delta G^\circ = 1.21\,\text{V} \tag{5}$$

$$CO_{2(g)} + 2H_2O_{(l)} \rightarrow CH_{4(g)} + 2O_{2(g)},$$
$$\Delta G^\circ = 818\,\text{kj/mol}, \quad \Delta E^\circ = 1.06\,\text{V}. \tag{6}$$

As shown in Fig. 1, the electrons are responsible for CO_2 reduction to convert it into low carbon fuels like CO and HCOOH, while on the other hand, holes in valance band interact with water molecules to produce O_2 [45].

In CO_2 photoreduction, the band gap holds great importance. The photoreduction takes place if the conduction band level is higher than that of reduction potential of CO_2, while valence band on the other hand is more positive than that of oxidation potential [45].

Photocatalytic properties arise when electron and hole charge carries are generated by absorbing incoming photons with energies equal or greater than that of band gap (E_g). Electrons in conduction band interact with H_2O to produce of H_2 and with CO_2 to produce other useful fuels [7, 16, 53, 54]. Many potential semiconductors have been studied based on this basic principle; some of them are TiO_2 [55, 56], ZnO [57–61], ZnS [61–64], $SrTiO_3$ [65–68], SiC [57, 69–71], Cu_2O [72–75], CdS [57, 76–81], GaP [57, 82], TaON [83–86], C_3N_4 [87–89], $BiVO_4$ [90–94], and Ta_3N_5 [95–98]. Among them, TiO_2 has been studied more because of its abundance, stability, photocatalytic activity, low toxicity, and versatility. One other main reason is it being primarily active under UV light due to its wide band gap, which

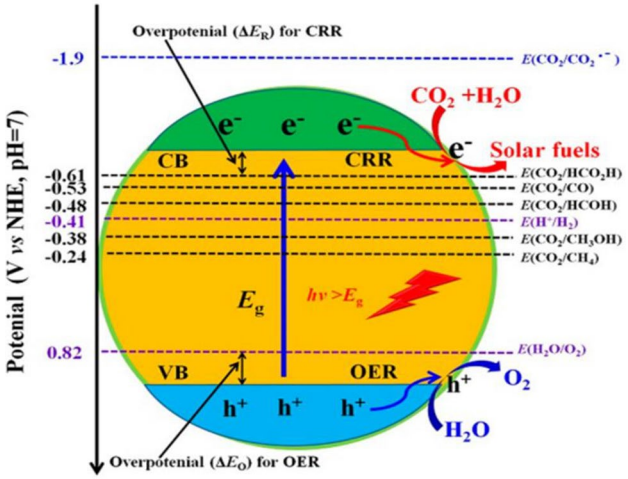

Fig. 1 Representation of CO_2 photoreduction in a semiconductor. Reprinted from [45, 52]

restricts its ability to absorb visible-light wavelength effectively [99–102]. The remaining materials are good photocatalyst for CO_2 photoreduction under visible light. These photocatalysts with more negative CB facilitates electron transfer and promote more efficient CO_2 conversion [4], as shown in Fig. 2.

An electrochemical reaction with higher standard potential is more thermodynamically favorable and tends to proceed in forward direction. Table 1 shows some of the electrochemical reactions with standard potential ΔE° at 25^0 C temperature and pH kept at 0. These data are further illustrated using graphical plot in Fig. 3. The standard potential provides insight into the spontaneity of the electrochemical process and its feasibility under standard conditions [103, 104].

3 Kinetic study of CO_2 photoreduction

The kinetics of CO_2 photoreduction is well explained by empirically derived Langmuir Hinshelwood model which also leads to micro-kinetic modeling [109]. The advantage of describing heterogeneous catalysis is it provision of insights into reaction mechanism, surface adsorption, the reaction rates at the catalyst surface, and the irradiance. Using this information, the rate of the reaction can be found using Eq. 1 [45]. The major flaw of this LH-based model is that it is time taking and much effort is needed in gathering the CO_2 photoreduction kinetics. Since heterogeneous catalytic reaction is majorly surface reactions, it is essential to determine the moles of reactants consumed or products generated per unit of time and per unit of reaction volume [109], while light is an additional requirement for some catalytic reaction.

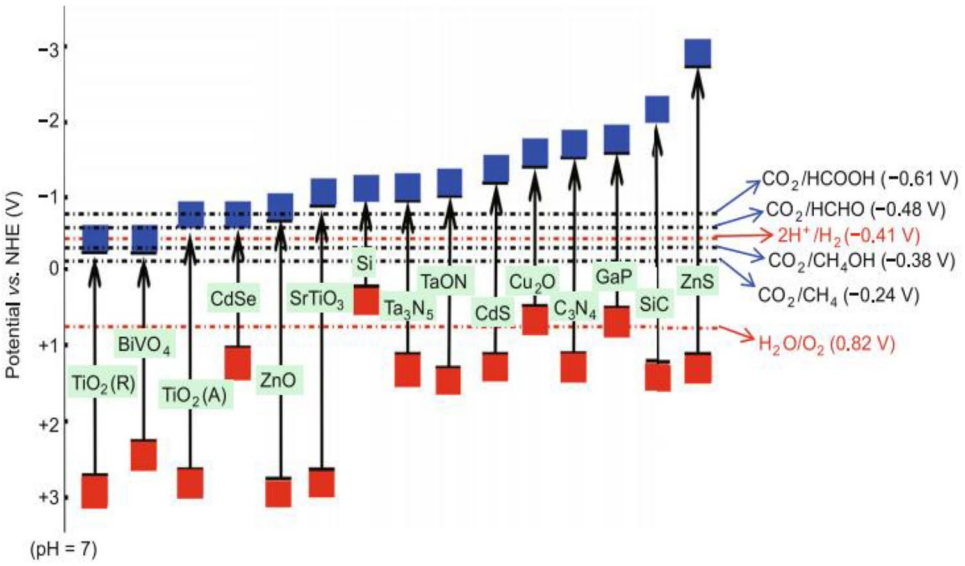

Fig. 2 Energy band characteristics in various semiconductors' photocatalysts and the redox potentials of CO_2 reduction in an aqueous solution pH = 7 [4]

Table 1 Standard potential for CO_2 reduction reaction [49, 105–108]

Electrochemical half-reaction	Standard potential ΔE°
$2H^+ + 2e^- \longrightarrow H_{2(g)}$	0
$2H_2O_{(l)} + 4h^+ \longrightarrow O_{2(g)} + 4H^+$	1.229
$CO_{2(g)} + e^- \longrightarrow CO_{2-}$	−1.9
$2CO_{2(g)} + 2H^+ + 2e^- \longrightarrow H_2C_2O_{4(aq)}$	−0.475
$CO_{2(g)} + 2H^+ + 2e^- \longrightarrow HCO_2H_{(l)}$	−0.2
$CO_{2(g)} + 2H^+ + 2e^- \longrightarrow CO_{(g)} + H_2O_{(l)}$	−0.12
$CO_{2(g)} + 4H^+ + 4e^- \longrightarrow C_{(s)} + 2H_2O_{(l)}$	0.21
$CO_{2(g)} + 4H^+ + 4e^- \longrightarrow HCHO_{(l)} + H_2O_{(l)}$	0.07
$CO_{2(g)} + 6H^+ + 6e^- \longrightarrow CH_3OH_{(l)} + H_2O_{(l)}$	0.03
$CO_{2(g)} + 8H^+ + 8e^- \longrightarrow CH_{4(g)} + 2H_2O_{(l)}$	0.17
$2CO_{2(g)} + 8H_2O_{(l)} + 12e^- \longrightarrow C_2H_{4(g)} + 12OH$	0.07
$2CO_{2(g)} + 9H_2O_{(l)} + 12e^- \longrightarrow C_2H_5OH_{(l)} + 12OH^-$	0.08
$2CO_{2(g)} + 13H_2O_{(l)} + 18e^- \longrightarrow C_3H_7OH_{(l)} + 18OH^-$	0.09

By maintaining both of these quantities, we can achieve the desired rate of reaction for CO_2 photoreduction

$$r = kI^{\alpha}\frac{\prod_{i=1}^{n} k_i p_i}{\left(1 + \sum_{i=1}^{z} k_i p_i\right)^n}. \tag{7}$$

Here, r is the rate of reaction (μmol $gcat^{-1}$ h^{-1}), k is the rate constant (μmol $gcat^{-1}$ h^{-1}), I is the irradiance, α is the reaction order of light intensity (dimensionless), k_i represents the equilibrium adsorption constants for reactants and product (bar^{-1}), p_i refers to partial pressures for reactants and products (bar), n indicates the absorbed reactants that are involved in surface reaction, and z indicates all the reactants and products [45]. Selectivity of catalyst is also based on temperature, because increasing the temperature also enhances the diffusion rate of molecules which directly impacts the rate of reaction [45]. LH-based kinetic model for CO_2 photoreduction is given by Fig. 3 [110–115].

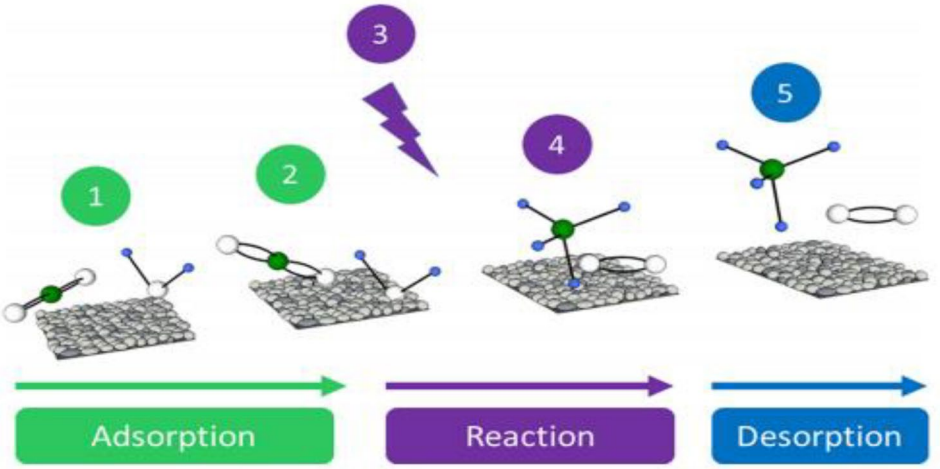

Fig. 3 Illustration of the Langmuir–Hinshelwood (LH)-based kinetic model for CO_2 photoreduction. [Step 1; H_2O and CO_2 diffuse to photocatalyst surface, step 2; molecules migrate within the active sites, step 3; light needed for rate of reaction, step 4; photoreaction start at active sites of two adjacent sites, Step 5; a the desired product is desorbed]

An LH-based model kinetics equation was developed for the gathering of the photoreduction catalysts for carbonate by UV/TiO_2 in aqueous solution [116]. Using UV light and TiO_2 to reduce carbonate in a solution is more effective when the solution is slightly acidic compared to when it is alkaline. The result also indicates that the speed at which this reduction happens increases when you have stronger UV light; however, adding too much TiO_2 actually blocks the UV light from penetrating the solution, as a result, slowing down the reaction [116, 117].

Hence, studies show that the photoreduction of CO_2 is thermodynamically favorable than that of kinetics photoreduction due to the context of multi-electron reduction processes [4], The efficiency of photocatalytic CO_2 reduction is influenced by factors such as the type of photocatalyst used, their band-gap energy, surface area, and structure of the crystal. Furthermore, several factors including lighting conditions (intensity, wavelength, and duration of illumination), along with reaction condition (temperature, pH), and co-catalyst enhance the photocatalytic efficiency. These factors improve adsorption, enable effective charge separation, and catalyze the conversion of reactants into valuable products. The choice of co-catalyst depends on the specific photocatalyst being used [118]. Basics of photocatalytic process can be summarized as follows:

(I) Photon is absorbed with sufficient energy which generates e^-/h^+ pairs.
(II) Separation of these charge carries and their transportation from valence band to conduction band.
(III) The occurrence of the chemical reaction on the surface [7, 119, 120].

The most frequently employed type of light is ultraviolet (UV) light source for photocatalysis, even though only 4% of solar energy is UV light, while 43% is visible light [121–123]. Hence, using narrow band photocatalyst in visible-light spectrum would be more energy efficient [124, 125].

The efficiency of a photocatalytic material can be calculated by its product yield. R can be given by

$$R = \frac{n(\text{Product})}{\text{Time} \times m(\text{catalyts})}.$$

The common unit for R is mol h^{-1} g^{-1} for the catalyst, while for the product, it is commonly measured in molar units (μmol) or in concentration units (ppm) [121]. The efficiency of photocatalyst depends upon the amount of photocatalyst, light intensity, the area exposed for their interaction, etc. The product which is formed by the photocatalyst can be measured by their quantum yield [121], using the formula below

$$\text{Overall quantum yield}\,(\%) = \frac{\text{Number of reactant electron}}{\text{Number of absorbed photon}} \times 100\%$$

$$\text{(App) quantum yield (QY\%)} = \frac{\text{Number of reactant electrons}}{\text{Number of incident photon}} \times 100\%$$

$$\text{(App) quantum yield of CO}\,(\%) = \frac{2 \times \text{Number of CO molecules}}{\text{Number of incident photons}} \times 100\%$$

$$\text{(App) quantum yield of HCOOH}(\%) = \frac{2 \times \text{Number of HCOOH molecules}}{\text{Number of incident photons}} \times 100\%$$

$$\text{(App) quantum yield of HCHO}\,(\%) = \frac{4 \times \text{Number of HCHO molecules}}{\text{Number of incident photons}} \times 100\%$$

$$\text{(App) quantum yield of } CH_3OH\,(\%) = \frac{6 \times \text{Number of } CH_3OH \text{ molecules}}{\text{Number of incident photons}} \times 100\%$$

$$\text{(App) quantum yield of } CH_4\,(\%) = \frac{8 \times \text{Number of } CH_4 \text{ molecules}}{\text{Number of incident photons}} \times 100\%.$$

As photocatalytic reaction strongly depends upon the photoabsorption, so the photocatalytic activity be contingent with the incident light wavelength. The quantum yield is calculated by calculating the intensity of light and amount of catalyst [126]. Experimental measurements required to determine the quantum yield for a photocatalytic process involving the production of carbon monoxide, formic acid, formaldehyde, methanol, and methane in a photocatalytic reaction are calculated. It is expressed as a percentage and is a measure of the efficiency of the process in converting absorbed photons into the formation of formic acid.

Numerous efforts have been dedicated to find suitable single-phase photocatalyst that can be driven by visible light (CdS [78, 81, 127], C_3N_4 [87, 128, 129], WO_3 [130, 131], $CaFe_2O_4$ [132], $LaCoO_3$ [133], $BiVO_4$ [134, 135], Bi_2WO_4 [136, 137], $Fe_2V_4O_{13}$ [138], and $InTaO_4$ [139–142] are active photocatalyst under visible region), and various strategies have emerged in the field of photocatalytic CO_2 reduction. These strategies include techniques like doping, alloying, utilizing surface plasmonic effects, introducing structural defects, sensitization, and forming solid solution [4, 143, 144]. Here, we will discuss two of these strategies, i.e., impurity doping and structural defects.

4 Impurity doping

To enhance the light-driven properties of utilizing semiconductors to enhance the photocatalytic reduction of CO_2, doping is the first strategic process which modulates the arrangement of electrons within a material, optical properties, and surface chemistry of the photocatalyst, leading to improved catalytic activity, selectivity, stability, and reduced energy barriers. Doping can be a versatile and effective strategy to customize the properties of photocatalysts for CO_2 reduction. The success of doping primarily hinges on the choice of dopants, dopants methods, and their potential impact on catalytic performance. Doping can create active sites on catalyst surface that facilitate CO_2 adsorption, activation, and reduction, enabling achievement of two-step photoexcitation using photons with low-energy visible-light spectrum [145, 146]. On the other hand,

nonmetal ion doping can shift the adsorption edge of the catalyst material toward longer wavelengths, enabling adsorption of visible light and that absorption is important for harnessing solar energy [147–149]. Nitrogen and iodine are well-studied material for their red shift optical behavior and they improve the visible-light absorption properties of wide-band-gap semiconductor materials [150]. TiO_2 is considered to be very prominent and potentially studied semiconductor material which has been investigated and developed [151]. Some important parameter for selectivity of the product includes temperature, pressure, and nature of the photocatalyst [152]. On the basis of these parameters, liquid-phase system is preferable. Many up-to-date research efforts have primarily focused on liquid samples, leaving the gas phase largely unexplored. This bias toward liquid-phase studies is often due to analytical limitations, as it is easier to analyze and quantify products in a liquid medium. However, this focus on liquid-phase studies has left the investigation of gas-phase products relatively neglected and less well understood. Gas phase system are reported solar products which are strongly dependent on the photocatalytic process, CO and CH_4 and their metal-doped properties are more functional for their production [153]. Among all metals, platinum (Pt) exhibits favorable results for methane due to higher surface electron density [154, 155]. Similarly, Cu [156], Ag [157], Ni [158], Mg [159], Au [160], Rh [161], and graphene [162] produce methane at a higher quantity in gas phase of CO_2 reduction. While in liquid-phase conversion of CO_2 reduction, the by-product is mostly methanol CH_3OH. Materials like Cu [115, 163], Ag [157], Ni [164, 165], Zn [166], and graphene-based material [167] are mostly studied broadly for their selectivity in photocatalytic Co_2 reduction, and their comparison is shown in Fig. 4.

The doping metal cations are more functional not only for creating space for active oxygen sites in reaction, but they are also for charge separation and adsorption through band-gap states. Contrary to this, we have to limit their concentration, because if dopant concentration increases, it will decrease the activity of photocatalytic CO_2 reduction.

5 Structural defects

Structural defects have crucial role in the photocatalytic CO_2 reduction process. These defects can include vacancies, interstitials atoms, grain boundaries, and other lattice imperfections in a photocatalytic material. Defects can impact the material's electronic structure, surface reactivity, and charge carrier dynamics. All of these factors play a vital role in facilitating the CO_2 reduction reaction. These defects introduce localized energy levels within the band gap of the material, promoting the absorption of a broader range of light wavelengths. An increased light absorption can improve the effectiveness of the photocatalytic process. Moreover, defects

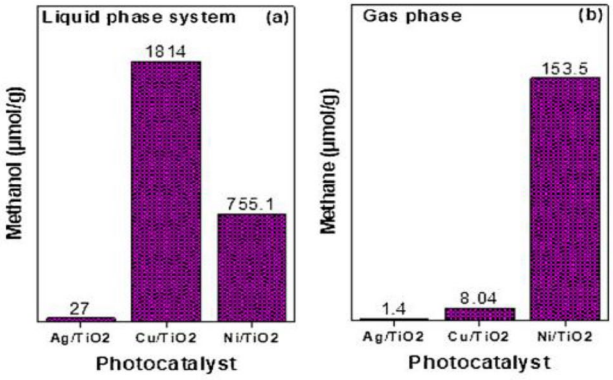

Fig. 4 Phase selectivity products in gas and liquid for CO_2 reduction [115, 152, 157, 160, 168, 169]

can assist as trapping sites for charge carriers, leading to prolonged lifetimes and improved segregation of electrons and holes, which is essential for redox reaction involved in CO_2 reduction. However, excessive defects might lead to an increased recombination of charge carrier, offsetting the beneficial effects [170–172].

Liu et al.[173] performed an investigation on the nanocrystals structure of TiO_2 and found that TiO_2 polymers can exhibit various crystalline configuration including (anatase, rutile, brookite, and TiO_2(B) polymorphs) [174]. It is worth noting that the formation of brookite is relatively infrequent or sporadic [175–177]. The photocatalytic CO_2 reduction is found to follow the sequence anatase > brookite > rutile [4]. Increase in generation of CO and CH_4 from CO_2 photoreduction in the existence of oxygen vacancies provides additional electronic states that can capture charge carriers (e^-/h^+) generated upon light absorption. Ti^{+3} species can act as electron donor, and its presence can also influence the charge carrier dynamics and surface activity, leading to an enhanced catalytic activity [173, 178]. Dislocations and grain boundaries are areas of crystal lattice mismatch within a material. These regions can create charge separation and accumulation zones, enchasing the disentanglement of photogenerated electron–hole pairs, as a result, charge carries can migrate to these regions and participate in CO_2 reduction reaction. Recognizing and addressing these defects through precise material design, controlled synthesis techniques, and innovative surface modification strategies are crucial steps toward maximizing the performance of photocatalytic CO_2 reduction.

Stimulated by the essential researches of CO_2 adsorption and dissociation at defect sites, incredible efforts have been done on the photocatalytic decrease of CO_2 by means of defect-mediated materials. For illustration, the co-exposed (001) and (101) facets of oxygen-deficient TiO2 nanocrystals were described to accomplish a quantum yield of 0.134% for CO_2 drop to CO underneath the expose of visible light [179,

180]. The electronic structure of catalyst is tuned by defect engineering, which extra advances the photocatalytic activity for the application of CO_2 reduction. For example, the defect-rich $BiVO_4$ nanosheets were produced and executed in CO_2 photoreduction. In the accumulation of vacancies persuaded by defects, the addition of interstitial and substitutional atoms into material lattice by doping [181]. The exotic atoms can be employed as active sites to alter the adsorption of CO_2 and related intermediates, forming various products. For illustration, it was described that the choosiness of CO_2 reduction could be mostly transformed by acquaint with various single-atom metal sites to g-C_3N_4 matrix.

6 Graphene-based nanomaterials

The initial isolation of graphene occurred and characterized in 2004 [182]. The diverse synthesis methods and distinctive characteristics of nanomaterials based on graphene make them highly favorable contender for the future technologies. Graphene is like a super-thin layer of sheets composed of carbon atom arranged in hexagonal pattern and incredibly thin that its thickness of only 0.334 nm which makes it the slenderest material globally. And because one of a kind properties like larger surface area (~ 2600 m^2/g) [183], higher electron mobility (200,000 cm^2/Vs) [184], escalate thermal conduction (3000–5000 Wm/K) [185], maximal optical transparency (97.4%) [186], and possessing remarkable strength characterized by a high young's modulus of 1TPa [187]. A carbon allotrope that exists primarily in a two-dimensional form composed of sp^2 carbon atom with hybridize orbitals is typically referred to as graphene (Fig. 5) by (Armano and Agnello) [188].

Apart from graphene, reduced graphene oxide (RGO), in addition to pure graphene, can serve as a viable material for CO_2 capture. When considering the production quantity, graphene oxide (GO) which is an intermediate product in graphene synthesis is also a valuable candidate. Between 2014 and 2022 in Fig. 6 [189], there has been remarkable threefold increase in the number of research publication focused on environmentally friendly methods for producing graphene from natural carbon resources.

Regarding the advancement of graphene, there have been significant development as considered a viable element for CO_2 capture application [190]. Graphene-based nanomaterials are the strongest cross-linking systems with strong light absorption and many functional groups. However, mass production of catalysts is still a challenge in terms of morphology, composition, and yield and cost control. This review provides an in-depth discussion of the combination of graphene with other nanomaterials, leading to new nanocomposites that can exhibit good properties such as rapid separation, transport, high surface area, and better CO_2 adsorption level. For charge transfer method heterojunctions, methods such as type II and type Z are common. In graphene heterojunctions, the graphene itself acts as electron tunneling, changing the Z type to the II type. Therefore, more attention should be paid to the Z shape of graphene-based nanomaterials (Table 2).

7 Summary and categories of graphene-based composite photocatalyst

Table 3 summarizes the graphene-based composite photocatalyst for CO_2 reduction. In summary, the main finding indicates that the graphene-based composite designed for reducing CO_2 through photocatalysis typically involves a combination of graphene and semiconductors. In this setup, semiconductor captures light energy, while graphene serves as a co-catalyst. Furthermore, there are reports indicating that substances derived from graphene, like graphene oxide (GO) and nitrogen-doped graphene, can act like semiconductors. These materials have been shown to effectively use light energy to reduce CO_2. Hence, they can be seen as a different category of photocatalyst based on derivatives of graphene.

The CO_2 transformation process comprises two essential steps: CO_2 capture and subsequent transport to the catalytic site [216, 217]. Porous capture materials are rich in adsorptive sites, yet they exhibit lower catalytic activity for CO_2 reduction compared to semiconductor or precious metals [218, 219]. Hence, the overall photoreduction efficiency is primarily contingent on the transfer of CO_2 from the capture materials to the photocatalyst [220]. Consequently, to attain greater CO_2 conversion rates, an effective photocatalyst must possess both a substantial CO_2 adsorption capacity and minimum diffusion distance. Creating a porous composites structure involves integrating hyper-crosslinked polymers (HCP) onto graphene functionalized with TiO_2 (TiO_2-FG) through an in situ knitting process. The HCPs, which constitute organic microporous materials in their pure form, exhibit a substantial surface area, exceptional CO_2 adsorption capacity, and remarkable physiochemical durability. Notability, this instance represents the integration of microporous organic polymers with photocatalyst for CO_2 conversion, a distractive approach amid the numerous reported photocatalytic methods. The TiO_2-G composite is first obtained through the reduction of graphene oxide (GO), followed by the in situ growth of anatase TiO_2 crystal featuring reactive [32, 215], via solvothermal process [221]. Ultra-thin polymer layer is hyper-crosslinked onto TiO_2-FG by knitting syn-$PhPh_3$ and connecting them to the open phenyl groups on graphene. This well-defined HCP-TiO_2-FG structure is expected to improve the adsorption capacity for CO_2 due to the enhanced characteristics of HCPs, and the short diffusion distance around the TiO_2 photocatalyst. This structure envisioned to boost

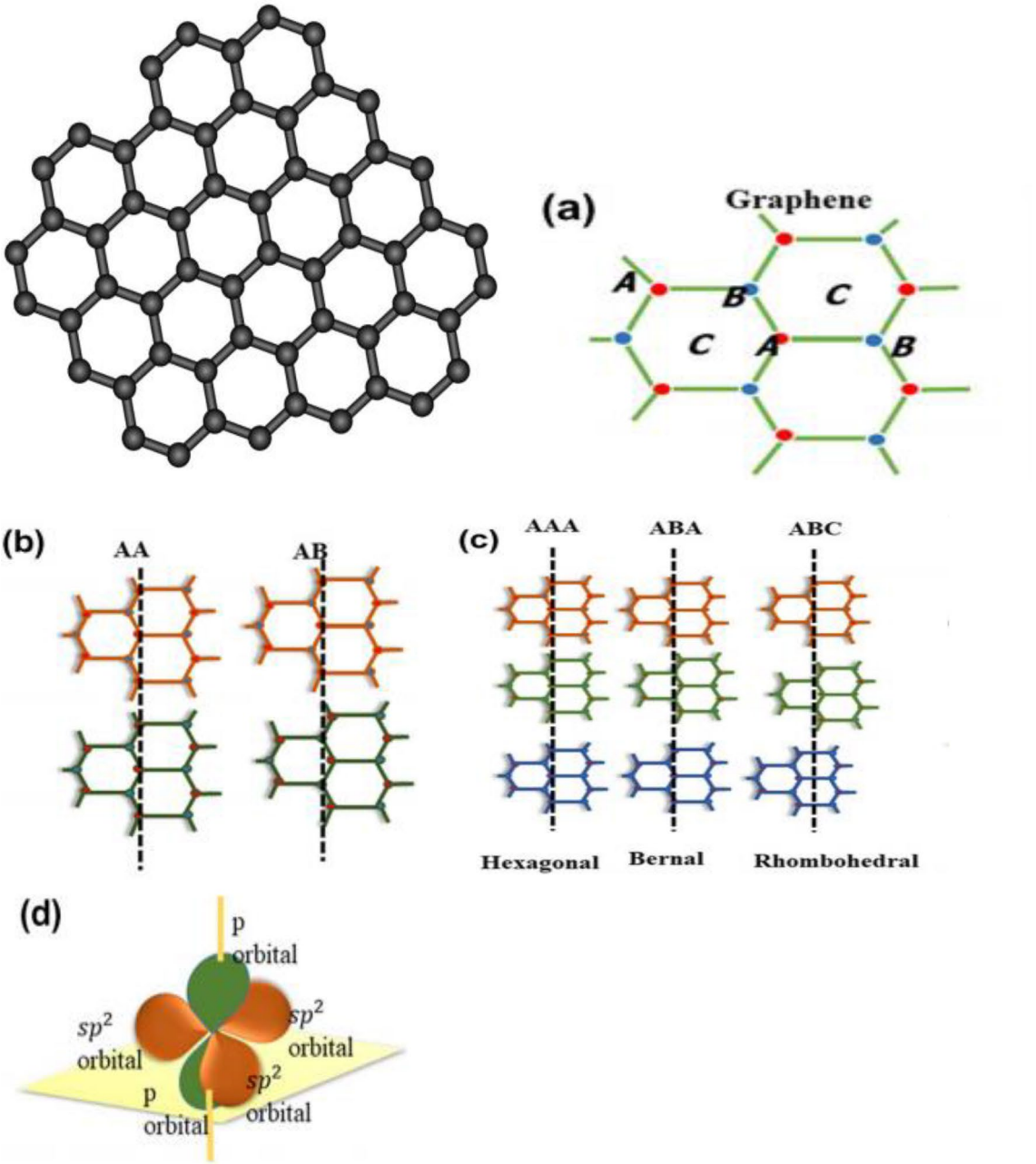

Fig. 5 Two dimensional structure of graphene: **a** SLG structure, A and B sublattice denotes carbon positions, **b** BLG stacking types, **c** TLG staking types, and **d** π covalent bond and sigma bond arrangement in the hexagonal lattice of graphene [186, 189]

the reactivity of CO_2 molecules, fascinating the production of CH_4. Well-defined structure is depicted in Fig. 7 [222].

Morphology of as above composites HCP-TiO_2-FG was inspected by FE-SEM, TEM, and atomic microscopy (AFM). Using FE-SEM analysis, we found that the pure HCPs, produced through our previous knitting technique, displayed structural layering within their bulk composition. In XRD, the samples compromised exclusively of anatase TiO_2 crystals. Incorporating HCPs layer did not induce any change in the crystal phase of TiO_2, but it did lead to a noticeable enlargement in the particular size in Fig. 8a, and the surface structure and composition is given by XPS measurement. In contrast to TiO_2-G, the strength of Ti and O signal peaks in TiO_2-FG and HCP-TiO_2-FG gradually diminished, primarily because of TiO_2 content. In high-resolution C1s spectra, the proportion of sp^2 and sp^3 signal exhibits an upward trajectory following the functionalizing and knitting. This change was attributed to an increase in the sp^2 presence in comparison

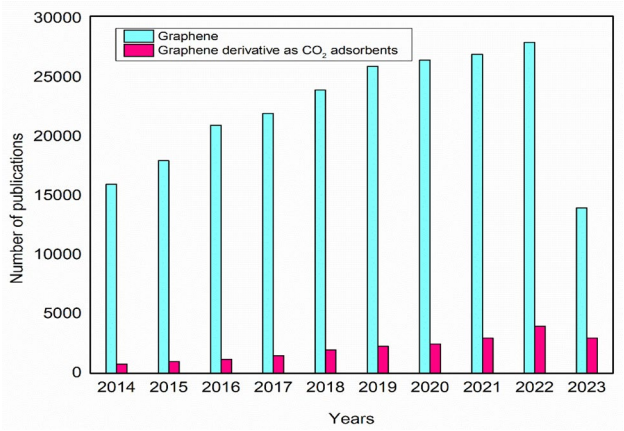

Fig. 6 Publication trends for graphene and its derivative over recent years [189]

to the generation of sp^3 C [223], as shown in Fig. 8b; notably, the peak of Ti2p experienced a shift of approximately (~ 0.2 eV) toward higher energy upon the creation of HCP layers. This electronic conformation shows the interaction between HCP and TiO_2. FT-IR spectrum of TiO_2-FG, the FT-IR spectrum of HCP-TiO_2-FG distantly exhibits pronounced C–H-stretching vibration of methylene around 2920 cm^{-1} and distinctive peaks related to the vibrations of the aromatic ring skeleton at approximately 1485 cm^{-1} [224, 225]. Incorporating phenyl groups into TiO_2-FG led to the emergence of supplementary peak at 136.7 ppm within the carbon region. This peak was attributed to the functionalization of TiO_2-G. Additionally, the resonance at 127.2 ppm was assigned to the sp^2 carbon of graphene. The increase intensity of resonance peak around 136.7 ppm can be attributed to the abundant introduction of sp^2 carbon through the process of knitting syn-phph3 with TiO_2-FG to create HCP-TiO_2-FG and simultaneously the formation of methylene with new peak at 32.9 ppm Fig. 8c [222]. The composite structure HCP-TiO_2-FG outstanding thermal stability even at temperature as high 400 °C due to presence of HCPs layers firmly on graphene. Porosity measurement is shown in Fig. 8d, both TiO_2 and TiO_2-FG shown IV isotherms, with less nitrogen adsorb quantity, these findings suggest limited surface area and the presence of mesoporous [226, 227]. The substantial specific surface area and the presence of numerous ultra-microspores in the HCP-TiO_2-FG composite have prompted us to explore its gas adsorption capabilities [228, 229]. Remarkably, HCP-TiO_2-FG exhibits CO_2 uptake, impressive 12.87% at 1 bar and 273.15 K, to contextualization these findings comparative analysis with various porous photocatalysts reported under analogues condition, as shown in Fig. 8e, f.

The integration of a semiconductor along with any photosensitizer or organic sacrificial reagent (Fig. 9a, b) shows the production CO_2 conversion products within a 5 h photocatalytic reaction, facilitated under visible-light condition ($\lambda = 420$ nm). Notably, this processes yielded the primary gases CO and CH_4, generated through 2e and 8e reduction processes [221]. The porous HCP-TiO_2-FG catalyst exhibited a notable average conversion efficiency at rate R_e of 264 μmol g^{-1} h^{-1}. Additionally, CH_4 and CO rates are 27.6 μmol g^{-1} h^{-1} and 21.63 μmol g^{-1} h^{-1}. Figure 9c shows as HCP-TiO_2-FG material displayed a remarkable 83.7% electron consumption selectivity for CH_4 production, while also effectively preventing H_2 evolution during the photocatalytic reaction. This underscores its high selectivity of CO_2 photoreduction and the undesired H_2O reduction. CO_2 conversion products were scarcely observed (< 1 μmol g^{-1} h^{-1}) in the case of commercial TiO_2 (P25) and pure TiO_2 featuring reactive (001) facets. This was primarily attributed to their constrained light absorption in the visible spectrum, in Fig. 9d. The combination of TiO_2 with graphene, resulting in TiO_2-G, and significantly enhanced CH_4 production (to 2.42 μmol g^{-1} h^{-1}) through the improvement of visible-light adsorption and electron transport properties [230–232]. Incorporating porous HCPs layers enriched the adsorption sites, leading to elevated CO_2 uptake and enhanced visible-light absorption [233]. Consequently, the creation of the well-structural HCP-TiO_2-FG composite significantly elevated the rate of photocatalytic CO_2 reduction. To assess the effectiveness of charge separation, transparent amperometric I–T curves were recorded during exposure to visible light. As shown in Fig. 9e, the resulting materials demonstrate excellent photocurrent stability throughout light on–off cycles, aligning consistently with the photocatalytic assessments. Notably, the pure TiO_2 system displayed a minimal signal, HCP-FG exhibits a weak photocurrent response, while the HCP-TiO_2-FG composites show better current intensity [234]. The route for charge carrier transfer and separation is typically contingent on the band gap of the photocatalyst [235]. HCP-FG exhibits its highest occupied molecular orbital (HOMO) and lowest unoccupied molecular orbital (LUMO) energy levels positioned at − 5.34 eV and − 3.00 eV verses vacuum level shown in Fig. 9d obtained by optical absorption. An overarching framework delineating the CO_2 conversion process over the HCP-TiO_2-FG photocatalyst is hereby put forth in Fig. 9f, and when exposed to visible-light irradiation, HCP-FG plays a dual role as a CO_2 adsorbent and a photosensitizer. It directly absorbs photons, thereby instigating the transition from the highest occupied molecular orbital (HOMO) to lowest unoccupied molecular orbital (LUMO) [236, 237].

Another brief mechanism for CO_2 reduction process over $CuInSnS_4$ a single metal sulfides, the context of this study, in situ Fourier-transform infrared spectroscopy is employed to analyze and contrast the reaction intermediates present on the catalyst surface [238]. No discernible macroscopic

Table 2 Summary of utilizing graphene and its derivative for CO_2 capture [191]

Material	Preparation method	Description precursor	Media	Physical properties	Chemical properties	Performance	References
Graphene	Thermal conversion	Nanodiamonds	1650 °C helium atmosphere	8–10 graphene layers, surface area: 280–1013 m^2/g	–	CO_2 adsorption: 10–38 wt% ($P=1$ atm, $T=195$ K)	[192]
	Thermal exfoliation	Graphite flake	1050 °C Argon atmosphere	3–4 graphene layer, surface area: 639–1550 m^2/g	–	CO_2 adsorption: 21–34 wt% ($P=1$ atm, $T=195$ K)	[192]
	Carbonization activation	Wood residue	KOH	Clear material voile like structure, surface area: 750–1735 m^2/g	FT-IR peaks: O–H, sp^3 and sp^2 CH, C=C, C–OH	Highest CO_2 adsorption capacity 12.68 mmol/g, ($P=10$ bar, $T=293$ K)	[193]
Graphene nanosheets	Modified hummer's method + ultrasonic dispersion	Graphite flake	H_2SO_4 $KmnO_4$ K_2FeO_4	Microspores, surface area: 284–964 m^2/g		1.14 mmol/g	[194]
		Solid wastes	H_2SO_4 $KmnO_4$ K_2FeO_4	Closely packed layer, microspores, surface area: 284–964 m^2/g	FT-IR peaks: C=O, aromatic C=C Carboxyl and epoxy C–O, NH_2, N–H, C–H	1.27–4.62 mmol/g	[194]
	Hummer's method	Graphite	H_2SO_4 $KmnO_4$ $NaNO_3$ H_2SO_4	Microspores, surface area: 284–964 m^2/g	–	1.08 mmol/g	[194]
	Thermal oxidative reduction	Graphite	H_3PO_4 $KmnO_4$ N_2H_4	Wrinkled and corrugated structure, surface area: 94–484 m^2/g	–	2.89 mmol/g ($P=1$ bar, $T=0$ °C)	[195]
Graphene Nanoplates	Vacuum-assisted thermal reduction	Graphite flakes	CH_3COOH $NaNO_3$ H_2SO_4 $KmnO_4$, 150–400 °C	Microspores, surface area: 151–324 m^2/g, larger interlayer spacing and higher interior void volume	–	Highest CO_2 capture capacity: 248 wt% ($P=30$ bar, $T=25$ °C)	[196]
Graphene oxide	Improved tour's method	Graphite flakes	H_2SO_4 H_3PO_4 $KmnO_4$	Agglomerates of graphene sheets, surface area: 9.08 m^2/g	FT-IR peaks: OH, C=O, C=C, C–O, $\frac{I_D}{I_G}$: 1.07	1.1 mmol/g ($P=1$ bar, $T=30$ °C)	[197]
Reduced graphene oxide	Reduction-induced self-assembly	Graphene oxide	Ascorbic acid (AsA)	In homogenous distribution of larger macroscopic pores and a more homogenous distribution of smaller pores, surface area: 60–328 m^2/g	–	2.1 mmol/g ($P=1$ atm, $T=25$ °C)	[198]

Table 3 A summary of the designing of graphene-based photocatalyst for CO_2 reduction [199]

Photoctalyst	Catalyst synthetic protocol	Light source	Experimental condition for CO_2 reduction	Product formed	Photocatalytic activity	References
GO	Hummer method + irradiation with solar & UV light	500W Xe lamp, stimulated sunlight; 4.5 h irradiation	CO_2 (100 mL min^{-1}	CO(Sunlight irradiation)	1.23 µmol g^{-1} h^{-1}	[200]
Cs_4PbBr_6/O/doped-rGO	Surfactant-mediated anti-solvent precipitation	300W Xe lamp	Ethyl acetate (5 mL)/DI H_2O (5 µL)	CO	11.4 µmol g^{-1} h^{-1}	[201]
In_2O_3/O/doped-rGO	Sol–gel	250W Hg vapor lamp	NaOH (2 M)/CO_2	CH_4	953.72 µmol g^{-1} h^{-1}	[202]
TiO_2/N/doped-rGO	Urea assisted hydrothermal	400 W Xe lamp	CO_2/H_2O (16 mL min^{-1})	CO	356.5 µmol g^{-1} h^{-1}	[203]
CdS/N/doped-rGO	Chemical vapor deposition	300W Xe lamp	CO_2/H_2O	CO and CH_4	CO(2.59) and CH_4 (0.33) µmol g^{-1} h^{-1}	[204]
Pt/Reduced Titania/N doped GO	Hydrothermal + photo deposition	100W Xe lamp	CO_2/H_2O (40 mL min^{-1})	CH_4	252 nmol g^{-1}	[205]
WSe_2/graphene/TiO_2	Ultrasonic techniques	500W Xe lamp;48 h reaction	Sacrificial reagent: $H_2O + Na_2SO_3$	CH_3OH	6.3262 µmol g^{-1} h^{-1}	[206]
ZnO/rGO	One-step hydrothermal	300W Xe lamp	1 M NaOH/CO_2	CH_3OH	263.17 µmol g^{-1}	[207]
TiO_2/rGO	Sonothermal–hydrothermal	8W UV lamp	ACN mixture (4:16 v/v)/TEOA	CH_3OH	2.33 mmol g^{-1} h^{-1}	[208]
Graphene/g-C_3N_4	Ultrasonic assisted + surface charge modification	15W daylight lamp; 10 h light irradiation	CO_2 (5 mL min^{-1})/H_2O	CH_4	13.93 µmol g^{-1}	[209]
Porous g- C_3N_4/graphene oxide	Hydrothermal co-assembly	500W Xe lamp; 6 h irradiation	MO solution used	CO	23 mmolg^{-1}	[210]
rGO/pg- C_3N_4	Ultrasonic assisted + surface charge modification	15W daylight lamp; 10 h light irradiation	CO_2 (5 mL min^{-1})/H_2O	CH_4	13.93 µmol g^{-1}	[211]
SiC/rGO	In-situ carbon template-deriving	300W arc lamp; 4 h irradiation	CO_2/H_2O (100 µL)	CH_4	58.17 µmol g^{-1} h^{-1}	[212]
ZnV_2O_6/rGO	One-pot solvothermal	35W HID Xe lamp; 10 h irradiation	100 mL H_2O + 0.1 M NaOH; CO_2 20 (mL/min)	CH_3OH, CH_3COOH and HCOOH	CH_3OH(5154), CH_3COOH(385.44 µmol g^{-1}), HCOOH(1942.41)	[213]
$CuCaAg_2Se$/TiO_2/GO	Muffled-assisted hydrothermal + pechini method	500W metal halide lamp; 48 h irradiation	Sacrificial scavenger: Na_2SO_4/50 mL DI water + $NaHCO_3$(0.04 M)	CH_3OH	Visible light:12.68%, UV light:16.84%	[214]
$LaYAgO_4$/TiO_2/GO	Hydrothermal	500W metal halide lamp; 48 h irradiation	Carbonated H_2O (50 mL)	CH_3OH	Visible light:1758.4, UV light:1945.9 mmol g^{-1}	[215]

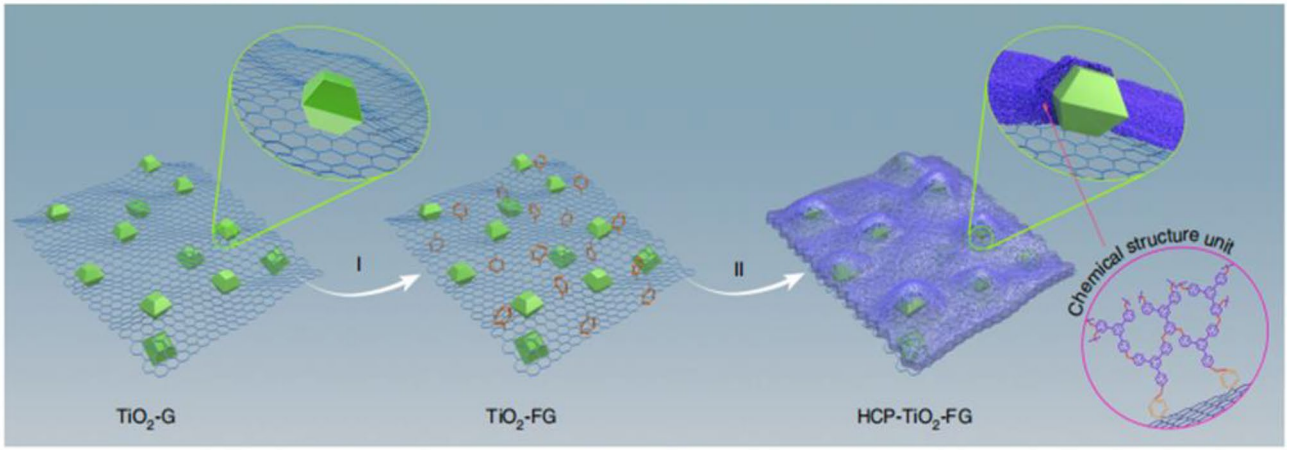

Fig. 7 (I) Enhancing the functionalization of TiO_2-G through the formation of Diazonium salts. (II) Merging TiO_2-FG with syn-$PhPh_3$ via solvent knitting technique. Upper right corner provide the detailed sectional view of the HCP-TiO_2-FG composite [221]

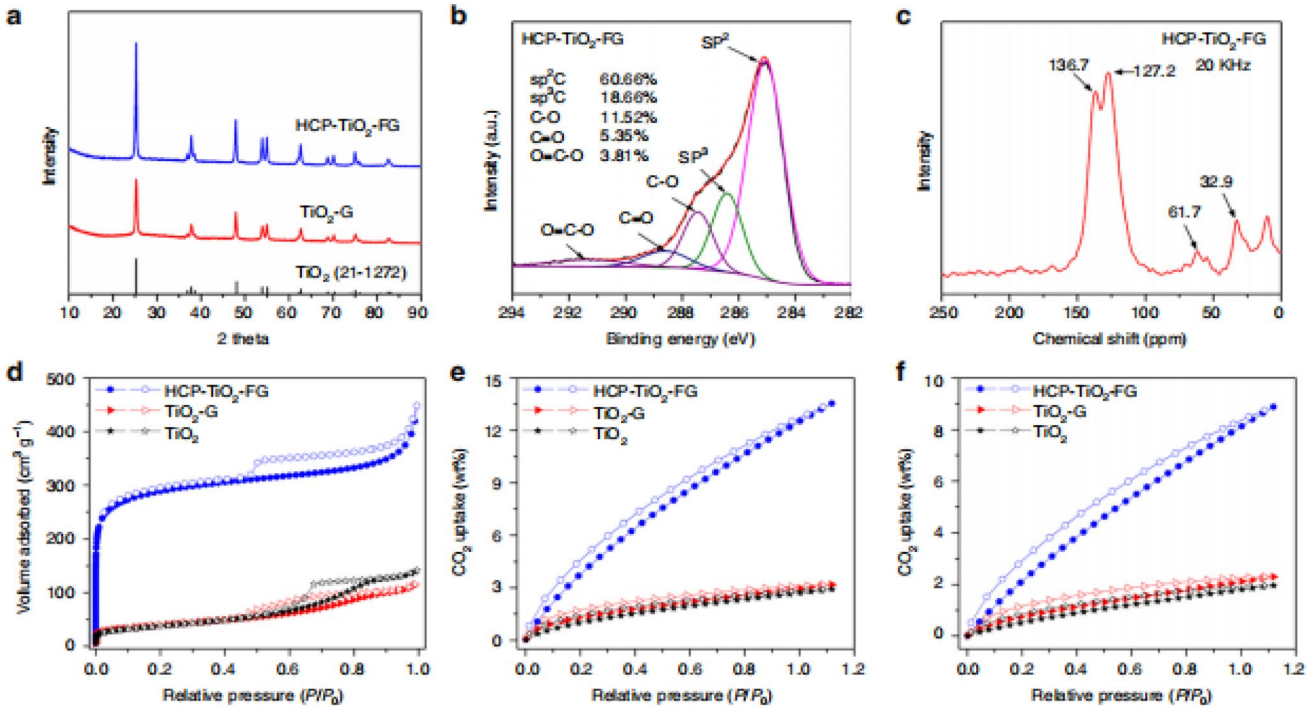

Fig. 8 Chemical composition, porous characteristics, and CO_2 adsorption capacity of different photocatalyst. **a** XRD image, **b** C^1 sketch HCP-TiO_2-FG, **c** C^{13} (CP/MAS), **d** N_2 adsorption at 77.3 K, and **e**, **f** volumetric CO_2 adsorption and desorption at 273.15 K and at 298.15 K for 1 bar [221]

infrared absorption peaks corresponding to reaction intermediate are observed on Cu_2S SnS_2 even in the presence of light irradiation. This absence may be attributed to their limited chemical interaction with CO_2 [239]. Conversely, In_2S_3 exhibits a pronounced activation effect on CO_2 adsorption at the surface when subjected to light irradiation [240] in Fig. 10a. Even in the absence of light, CO_2 chemisorbs onto In_2S_3 evident from the 1150 cm^{-1} IR peak denoting an O–S-stretching vibration [241], sufficient oxygen–sulfur bonding. The oxygen atom of CO_2 is chemically linked to the sulfur atom of In_2S_3 [242]. Under light exposure, specific infrared peaks on the catalyst surface are detected. 1225 cm^{-1} peak corresponding to bidentate bicarbonates vibrations, while the 1412 cm^{-1} peaks signifies monodentate bicarbonates

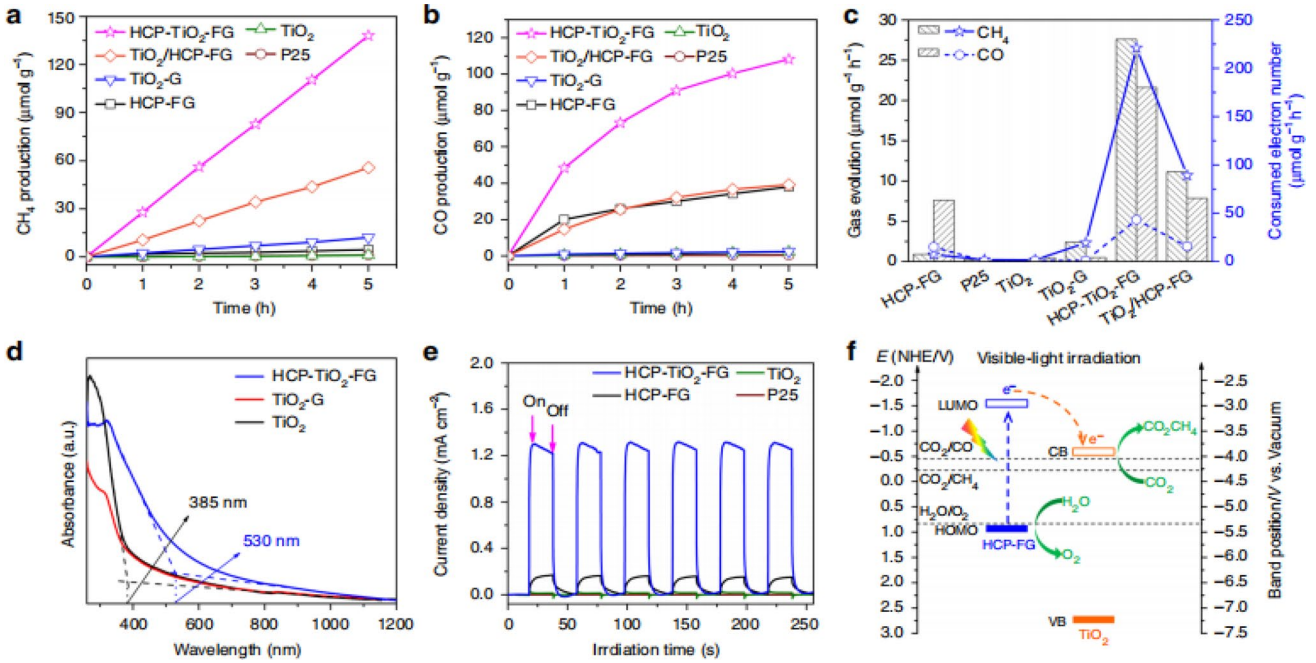

Fig. 9 The photoreduction of CO_2, optical and photoelectrical characteristics, and the intricacies of the charge transfer pathways all contribute to the assessment of the photocatalytic efficiency, specifically: **a** CH_4 and **b** CO in the context of photocatalytic CO_2 reduction, **c** average conversion efficiency rate of CH_4 and CO, **d** UV absorption of catalyst, **e** amperometric I–T curve of sample, and **f** suggested mechanism of charge separation and transfer in the composite photocatalyst HCP-TiO_2-FG [221]

vibration [243]. Of particular significance, the 1610 cm^{-1} peak is associated with the *COOH group, a critical intermediate in the CO_2 reduction to CO process. Remarkably, the polymetallic sulfide $CuInSnS_4$ displays robust CO_2 chemisorption and substantial H_2O physisorption (Fig. 10b).

The CO_2 adsorption configuration on $CuInSnS_4$ is pivotal in determining its outstanding CO_2 photoreduction activity and selectivity. To investigate the CO_2 conversion pathways on the $CuInSnS_4$ photocatalyst surface, DFT calculation were conducted, as shown in Fig. 11.

The adsorption arrangement of $CuInSnS_4$ is illustrated for each for each incremental step, encompassing CO_2 adsorption through CH_4 generation. Various intermediate states, including CO_2*, COOH, CHO*, CH_2O*, and CH_3* and their corresponding C atom are depicted which consistently maintain strong bonds with electron-deficient sulfur atoms on the (111) plane of the $CuInSnS_4$ nano-signal crystal.

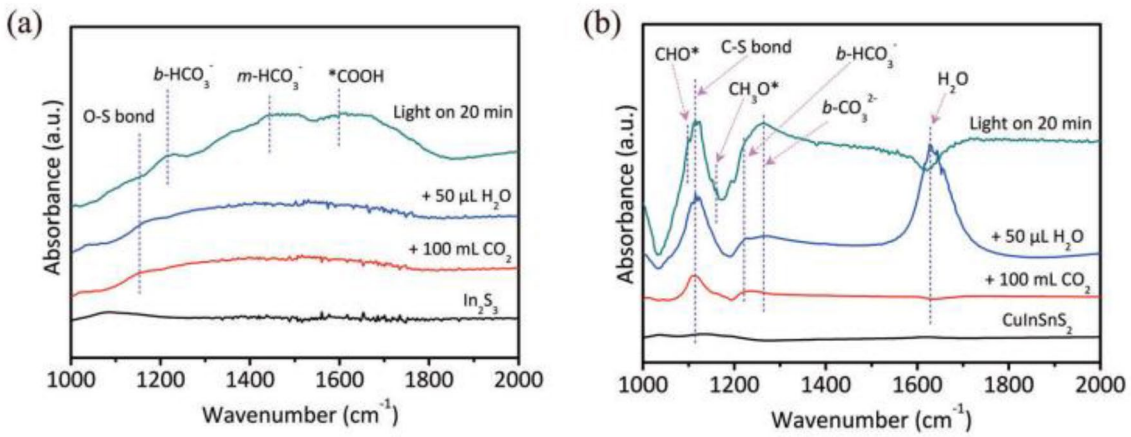

Fig. 10 In-situ FT-IR spectra for adsorbed CO_2: **a** In_2S_3 and **b** $CuInSnS_4$ [238]

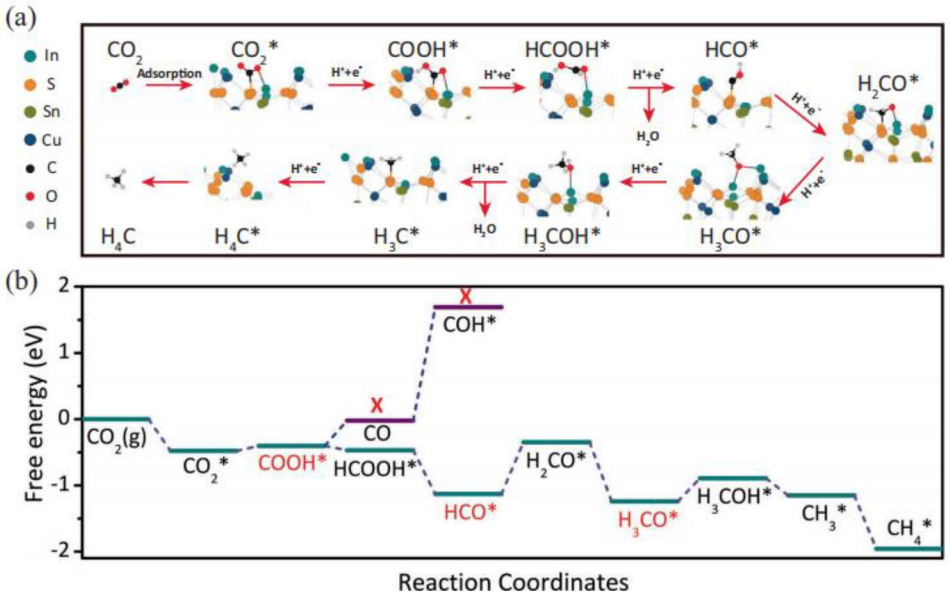

Fig. 11 **a** Calculate adsorption configuration of CO_2 & reactive on $CuInSnS_4$, and **b** Gibbs free energy of CO_2 to CH_4 [238]

8 Advantages of using carbon materials for CO_2 reduction

Using carbon materials in photocatalytic reaction has advantages like providing more spaces for reactions, making CO_2 easier to work with, separation of charges and absorbing more light energy for better performance. Materials made from carbon, like graphene oxide, graphene, carbon nanotubes (CNTs), and g-C_3N_4, offer an expanded surface area of the catalyst, when they are combined [244]. g-C_3N_4 has many imperfections on its surface, because it contains hydrogen atoms and has an abundance of electrons. These imperfections make it useful for catalytic reactions as they help electrons move around more easily on the surface of catalyst. Yang et al. created nanosheets made of NiAl-layered double hydroxide (NALDH). They then joined these nanosheets with g-C_3N_4 nanosheets and observed a very closed connection between the two nanosheets, forming a strong heterojunction [245, 246]. Additionally, they include graphene aerogels, which played a role in extending the structure into network-like structure. In this research, they used both graphene nanosheets as well as aerogels to enhance the performance of the photocatalyst. Creating these extremely close connections between sheets reduced the distance for the conveyance of electric charges and also gave plenty of active sites for chemical reaction to occur. Using N_2 adsorption–desorption measurements, a significant enhancement in the specific surface area and pore volume was determine over a broad range, as shown in Fig. 12a [247]. In recent work by Chen et al. combined porous carbon nanofiber with added nitrogen with the mixture of nickel and molybdenum phosphide (Mo/Ni-PS@PAN), they used a method involving phosphatization to make the catalyst particular larger, increasing their size from 20 to 50 nm. They conducted carbonization to further enlarge the size. When nanoparticles of MoP were mixed with evenly spread-out nickel atoms, it produced a material known as NiMoP@NCPF, through the process of carbonization the size expend from 50 to 100 nm, as shown in Fig. 12b, c. The porous structure of the material they obtained played a pivotal role in enhancing CO_2 adsorption while carrying out the photocatalytic reduction reaction as indicated in Fig. 12d [248].

Apart from the characteristic of pore structures, the way gases interact with the surface is also vital for CO_2 adsorption. Therefore, when we modify the surface of carbon materials, we can make CO_2 molecules more polar and thus enhance their adsorption. This is achieved by incorporating the fundamental functional group within the carbon framework [249–251]. Various forms of carbon materials have been utilized as support materials for the photoreduction of CO_2. Carbon-based materials hold tremendous promise for their high efficiency in CO_2 adsorption to their adjustable structure and ample surface area [252]. As g-C_3N_4, it can have a substantial surface area. In certain instance, graphene materials can be modified by adding protons, utilizing substances that protonate to boost area of interest. In recent research, Wu et al. conducted innovative research where they used g-C_3N_4 as a template. They created layer of g-C_3N_4 and introduced a combination of Ni/Co metal into the empty spaces within g-C_3N_4 using phosphoric acid [253–255]. With the addition different amounts metal dopants, it caused a transformation in the microstructure leading the formation of g-C_3N_4-Ni-Co with various sizes, as shown in Fig. 13a–c. And by adding bimetallic dopant will create more hole in g-C_3N_4 which increase the nitrogen vacancies [256]. Figure 13d shows the

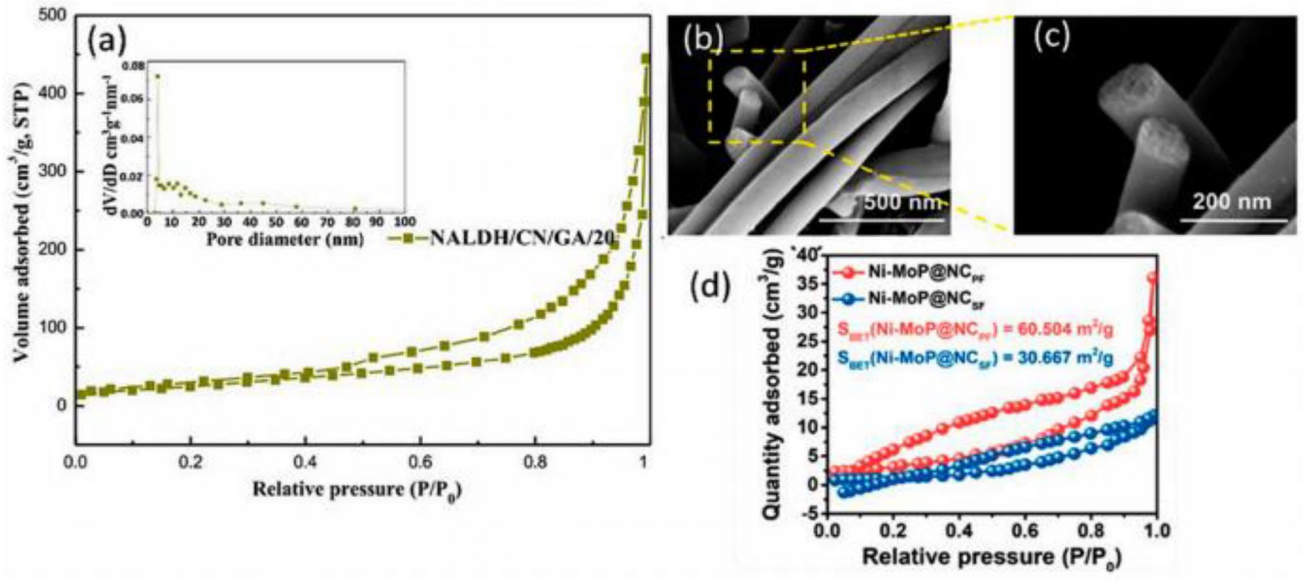

Fig. 12 **a** N_2 adsorption and desorption curves and the accompanying image depicting pore size spread image of NALDH. Reproduced with the permission from reference [247]. **b**, **c** SEM image of NiMoP@NCPF, and **d** BET (Brunauer–Emmett–Teller) of NiMoP@NCPF and NiMoP@NCSF [248]

catalyst activity at different proportions and the by-product is formed is CO, the porous structure provides numerous spots and a broad catalytic surface area, speeding up the reaction. As a result, this significantly boost the CO production rate to 13.51 mmol/g/h, which is surpassing the achieved value by a factor 3.9 times, with g-C_3N_4, as shown in Fig. 13e [257].

Numerous research articles have been extensively explored the field of CO_2 photoreduction, with semiconductor like TiO_2 emerging as the promising candidates for achieving reliable results. Despite notable achievements in this area, several challenges persist in the development of semiconductor photocatalyst, including low thermal and chemical stability, and reduced efficiency under specific conditions. In contrast, polymeric materials exhibit range of appealing characteristics, including cost-effectiveness, low toxicity, widespread availability, and light weight nature, ease of synthesis and use, and excellent flexibility [258, 259]. g-C_3N_4 stands out as an appealing polymeric photocatalyst, demonstrating superior performance even without the need for need metal composites of noble metal. In polymeric materials, the production of (e^-) and (h^+) pairs occurs more rapidly compared to semiconductor photocatalyst like g-C_3N_4, primarily due to the presence of piled π bonds [260–263]. These accumulated π bonds within polymers facilitate instant charge transfer processes, as they were well candidates for catalyzing the CO_2 photocatalytic reduction [260, 264–267]. The role of these stacked π bonds in CO_2 photoreduction is significant, although research in this area for π conjugated materials are is still in its nascent stages. These stacked π bonds can play a pivotal role in the photoreduction of CO_2; however, research on π conjugated materials is still in nascent stages [258].

Intensified research into polymeric materials derived from carbon holds greater promise for enhancing the photocatalytic reduction of CO_2 when compared to current semiconductor photocatalyst. While these promising materials have shown favorable outcomes, further adjustments and the fine-tuning of band gaps are essential to achieve optimal results. It is crucial to consider both materials design and reaction methodology in this context. However, equally significant is evaluating the overall performance and sustainability of the entire energy generation and conversion process. With the aim of producing environmentally friendly fuels and mitigating the greenhouse effect in the future, it necessitates a more through and expansive investigation. This entails employing advanced tools and conducting detailed studies to gain a deeper understanding of these reaction [267–270].

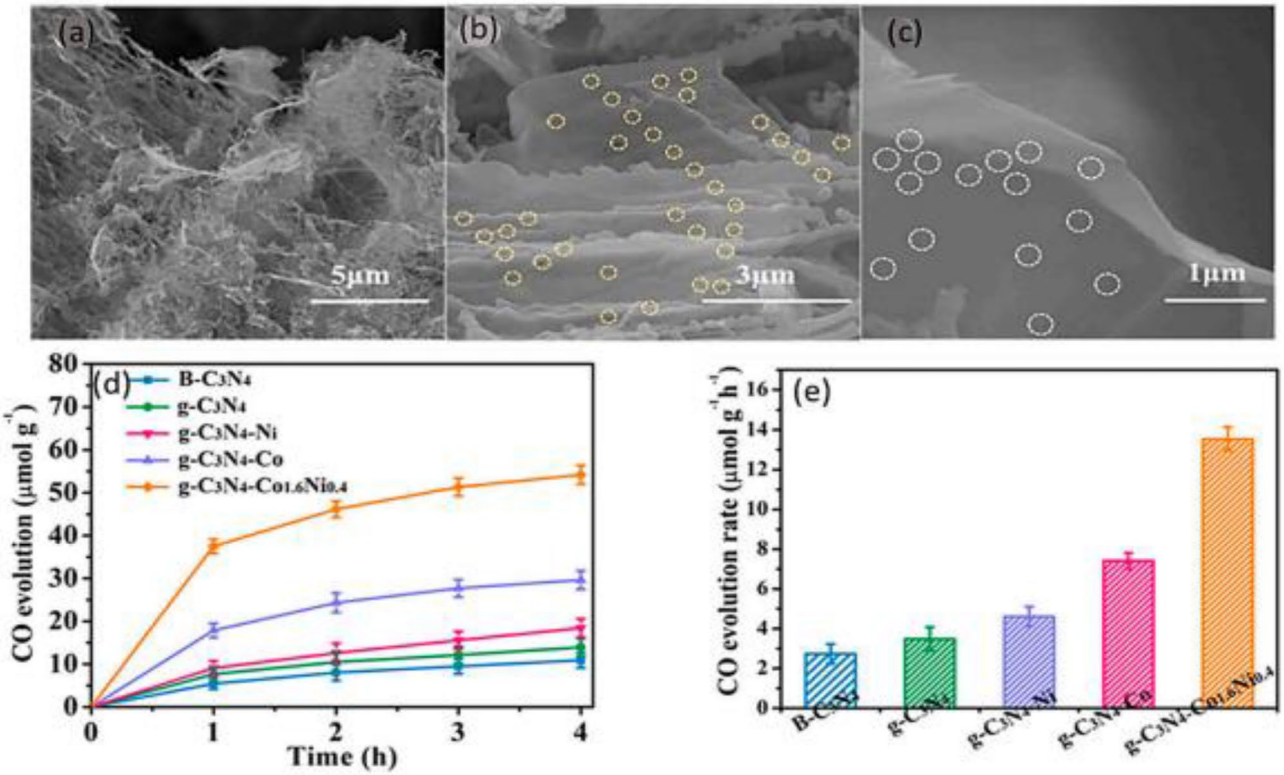

Fig. 13 **a**–**c** SEM visual representation of g-C_3N_4-$Co_{1.6}$-$Ni_{0.4}$ in various sizes, **d** CO generation time, and **e** CO production rate g-C_3N_4–Co_x-Ni_y [257]

9 Conclusion

In a global context increasingly oriented toward sustainable solutions, photocatalytic carbon dioxide photoreduction emerges as a pioneering innovation, presenting a promising avenue for addressing carbon emissions. By leveraging the transformative potential of light to convert carbon dioxide into valuable resources, this approach not only tackles environmental challenges but also unveils a spectrum of possibilities for cleaner energy and greener technologies. This comprehensive review primarily centers on elucidating the factors influencing product outcomes in CO_2 photoreduction.

CO_2 photoreduction, while holding promise as a sustainable approach for mitigating carbon emissions, confronts several challenges. The primary hurdle lies in the inherently low efficiency of the photoreduction process due to the limited absorption of solar radiation by CO_2 and the competitive reduction of protons to hydrogen. Furthermore, a significant challenge is the selectivity toward desired products, often resulting in the generation of undesired by-products. Product distribution forms the basis for tailoring catalyst yield of desired products, emphasizing the necessity of achieving a delicate equilibrium between product selectivity and overall process efficiency. Thermodynamic considerations, such as redox potential and Gibbs free energy, offer insights into the energy requirements and feasibility of the process, predicting electron pathways and routes for optimal conditions conducive to efficient CO_2 reduction. Additionally, the adsorption and CO_2 activation properties eliminate product oxidation, maximizing efficiency. This implies that a purposefully engineered semiconductor with an enhanced adsorption ratio facilitates reaction kinetics.

Optimizing the compositional balance between these factors, although challenging, is essential for achieving high efficiency in CO_2 photoreduction, necessitating further modifications. To ascertain production yield, differentiation between derivation from CO_2 and impurities is imperative, achievable through isotope labeling in nano-scale probes.

To address the challenges involved in engineering of photocatalytic materials with enhanced properties' development of innovative reactor system is crucial. Perspective solutions involve the engineering of photocatalytic materials with enhanced light absorption properties and tailored catalytic sites for improved selectivity. Integration of tandem catalysis, wherein multiple catalytic processes are sequentially coupled, may further enhance overall efficiency. Future strategies should focus on the exploration of novel materials, such as semiconductor nanomaterial and molecular catalysts, and

the implementation of advanced computational approaches to guide catalyst design. Concurrently, a thorough investigation into photostability is imperative. The development of a robust and stable photocatalytic system capable of sustained operation under diverse conditions remains a critical objective. Additionally, efforts toward understanding the fundamental mechanistic aspects of CO_2 photoreduction will be pivotal for optimizing and scaling up this technology to contribute substantively to carbon management and sustainable energy systems.

Declarations

Conflict of interest The authors declare that there is no conflict of interest regarding the publication of this paper.

References

1. J. Ma, N. Sun, X. Zhang, N. Zhao, F. Xiao, W. Wei, Y. Sun, A short review of catalysis for CO_2 conversion. Catal. Today **148**, 221–231 (2009)
2. Z. Sun, J. Dong, C. Chen, S. Zhang, Y. Zhu, Photocatalytic and electrocatalytic CO_2 conversion: from fundamental principles to design of catalysts. J. Chem. Technol. Biotechnol. **96**, 1161–1175 (2021)
3. S. Zhang, Q. Fan, R. Xia, T.J. Meyer, CO_2 reduction: from homogeneous to heterogeneous electrocatalysis. Acc. Chem. Res. **53**, 255–264 (2020)
4. X. Li, J. Wen, J. Low, Y. Fang, J. Yu, Design and fabrication of semiconductor photocatalyst for photocatalytic reduction of CO_2 to solar fuel. Sci. China Mater. **57**, 70–100 (2014)
5. A.J. Bard, M.A. Fox, Artificial photosynthesis: solar splitting of water to hydrogen and oxygen. Acc. Chem. Res. **28**, 141–145 (1995)
6. M.G. Walter, E.L. Warren, J.R. McKone, S.W. Boettcher, Q. Mi, E.A. Santori, N.S. Lewis, Solar water splitting cells. Chem. Rev. **110**, 6446–6473 (2010)
7. X. Chen, S. Shen, L. Guo, S.S. Mao, Semiconductor-based photocatalytic hydrogen generation. Chem. Rev. **110**, 6503–6570 (2010)
8. D. Cheng, H.H. Ngo, W. Guo, S.W. Chang, D.D. Nguyen, Y. Liu, X. Zhang, X. Shan, Y. Liu, Contribution of antibiotics to the fate of antibiotic resistance genes in anaerobic treatment processes of swine wastewater: a review. Biores. Technol. **299**, 122654 (2020)
9. S. Dahl, I. Chorkendorff, Towards practical implementation. Nat. Mater. **11**, 100–101 (2012)
10. V.N.H. Nguyen, T.H. Nguyen, M.S. Lee, Review on the comparison of the chemical reactivity of Cyanex 272, Cyanex 301 and Cyanex 302 for their application to metal separation from acid media. Metals **10**, 1105 (2020)
11. S. Lingampalli, M.M. Ayyub, C. Rao, Recent progress in the photocatalytic reduction of carbon dioxide. ACS Omega **2**, 2740–2748 (2017)
12. S. Sato, T. Arai, T. Morikawa, K. Uemura, T.M. Suzuki, H. Tanaka, T. Kajino, Selective CO_2 conversion to formate conjugated with H_2O oxidation utilizing semiconductor/complex hybrid photocatalysts. J. Am. Chem. Soc. **133**, 15240–15243 (2011)
13. S.-Y. Liu, A. Zada, X. Yu, F. Liu, G. Jin, $NiFe_2O_4$/g-C_3N_4 heterostructure with an enhanced ability for photocatalytic degradation of tetracycline hydrochloride and antibacterial performance. Chemosphere **307**, 135717 (2022)
14. Z. Liao, Y. Wu, S. Cao, S. Zhao, X. Yan, S. Yuan, K. Dong, J. Qin, C. Ou, J. Zhu, Facile engineering of PES ultrafiltration membranes using polyoxometalates for enhanced filtration and antifouling performance. Sep. Purif. Technol. **308**, 122911 (2023)
15. A. Kudo, Y. Miseki, Heterogeneous photocatalyst materials for water splitting. Chem. Soc. Rev. **38**, 253–278 (2009)
16. K. Maeda, K. Domen, New non-oxide photocatalysts designed for overall water splitting under visible light. J. Phys. Chem. C **111**, 7851–7861 (2007)
17. P. Dhull, A. Sudhaik, V. Sharma, P. Raizada, V. Hasija, N. Gupta, T. Ahamad, V.-H. Nguyen, A. Kim, M. Shokouhimehr, An overview on $InVO_4$-based photocatalysts: electronic properties, synthesis, enhancement strategies, and photocatalytic applications. Mol. Catal. **539**, 113013 (2023)
18. N. Shehzad, M. Tahir, K. Johari, T. Murugesan, M. Hussain, Improved interfacial bonding of graphene-TiO_2 with enhanced photocatalytic reduction of CO_2 into solar fuel. J. Environ. Chem. Eng. **6**, 6947–6957 (2018)
19. L. Wei, C. Yu, Q. Zhang, H. Liu, Y. Wang, TiO_2-based heterojunction photocatalysts for photocatalytic reduction of CO_2 into solar fuels. J. Mater. Chem. A **6**, 22411–22436 (2018)
20. J. Cai, F. Shen, Z. Shi, Y. Lai, J. Sun, Nanostructured TiO_2 for light-driven CO_2 conversion into solar fuels. APL Mater. **8**, 1 (2020)
21. X. Yu, V.V. Ordomsky, A.Y. Khodakov, Selective deposition of cobalt and copper oxides on $BiVO_4$ facets for enhancement of CO_2 photocatalytic reduction to hydrocarbons. ChemCatChem **12**, 740–749 (2020)
22. X. Wang, Y. Wang, M. Gao, J. Shen, X. Pu, Z. Zhang, H. Lin, X. Wang, $BiVO_4$/$Bi_4Ti_3O_{12}$ heterojunction enabling efficient photocatalytic reduction of CO_2 with H_2O to CH_3OH and CO. Appl. Catal. B **270**, 118876 (2020)
23. X. Li, D. Wei, L. Ye, Z. Li, Fabrication of Cu_2O-RGO/$BiVO_4$ nanocomposite for simultaneous photocatalytic CO_2 reduction and benzyl alcohol oxidation under visible light. Inorg. Chem. Commun. **104**, 171–177 (2019)
24. B. Han, X. Ou, Z. Deng, Y. Song, C. Tian, H. Deng, Y.J. Xu, Z. Lin, Nickel metal–organic framework monolayers for photoreduction of diluted CO_2: metal-node-dependent activity and selectivity. Angew. Chem. Int. Ed. **57**, 16811–16815 (2018)
25. K. Song, X. Qiu, B. Han, S. Liang, Z. Lin, Efficient upcycling electroplating sludge and waste PET into Ni-MOF nanocrystals for the effective photoreduction of CO_2. Environ. Sci. Nano **8**, 390–398 (2021)
26. H.-N. Wang, H.-X. Sun, Y.-M. Fu, X. Meng, Y.-H. Zou, Y.-O. He, R.-G. Yang, Varied proton conductivity and photoreduction CO_2 performance of isostructural heterometallic cluster based metal–organic frameworks. Inorgan. Chem. Front. **8**, 4062–4071 (2021)
27. M. Que, Y. Zhao, Y. Yang, L. Pan, W. Lei, W. Cai, H. Yuan, J. Chen, G. Zhu, Anchoring of formamidinium lead bromide quantum dots on Ti_3C_2 nanosheets for efficient photocatalytic reduction of CO_2. ACS Appl. Mater. Interfaces **13**, 6180–6187 (2021)
28. K. Ren, S. Yue, C. Li, Z. Fang, K.A. Gasem, J. Leszczynski, S. Qu, Z. Wang, M. Fan, Metal halide perovskites for photocatalysis applications. J. Mater. Chem. A **10**, 407–429 (2022)
29. S. Park, S. Choi, S. Kim, K.T. Nam, Metal halide perovskites for solar fuel production and photoreactions. J. Phys. Chem. Lett. **12**, 8292–8301 (2021)
30. Y. Cui, P. Ge, M. Chen, L. Xu, Research progress in semiconductor materials with application in the photocatalytic reduction of CO_2. Catalysts **12**, 372 (2022)
31. R. Sharma, M. Khanuja, S.N. Sharma, O.P. Sinha, Reduced band gap & charge recombination rate in Se doped α-Bi_2O_3 leads to enhanced photoelectrochemical and photocatalytic performance:

theoretical and experimental insight. Int. J. hydrog. Energy **42**, 20638–20648 (2017)
32. J. Xiong, M. Zhang, M. Lu, K. Zhao, C. Han, G. Cheng, Z. Wen, Achieving simultaneous Cu particles anchoring in mesoporous TiO_2 nanofabrication for enhancing photo-catalytic CO_2 reduction through rapid charge separation. Chin. Chem. Lett. **33**, 1313–1316 (2022)
33. H. Yu, J. Huang, L. Jiang, X. Yuan, K. Yi, W. Zhang, J. Zhang, H. Chen, Steering photo-excitons towards active sites: intensified substrates affinity and spatial charge separation for photocatalytic molecular oxygen activation and pollutant removal. Chem. Eng. J. **408**, 127334 (2021)
34. F. Khodabandeloo, S. Shahsavarifar, B. Nayebi, K.P. Niavol, B. Nayebi, R.S. Varma, J.H. Cha, H.W. Jang, D. Kim, M. Shokouhimehr, Applications of nanostructured semiconductor photocatalysts for the decontamination of assorted pollutants from wastewater. Inorgan. Chem. Commun. **2023**, 111357 (2023)
35. M. Zhu, X. Zhang, H. Feng, J. Dai, J. Li, Q. Che, Q. Gu, T. Zhu, D. Li, Penicisulfuranols A–F, alkaloids from the mangrove endophytic fungus *Penicillium janthinellum* HDN13-309. J. Nat. Prod. **80**, 71–75 (2017)
36. H. Maleki-Ghaleh, M. Shakeri, Z. Dargahi, M. Kavanlouei, H.K. Garabagh, E. Moradpur-Tari, A. Yourdkhani, A. Fallah, A. Zarrabi, B. Koç, Characterization and optical properties of mechanochemically synthesized molybdenum-doped rutile nanoparticles and their electronic structure studies by density functional theory. Mater. Today Chem. **24**, 100820 (2022)
37. N.U.M. Nor, E. Mazalan, C. Risko, M. Crocker, N.A.S. Amin, Unveiling the structural, electronic, and optical effects of carbon-doping on multi-layer anatase TiO_2 (1 0 1) and the impact on photocatalysis. Appl. Surf. Sci. **586**, 152641 (2022)
38. C. Feng, Z. Chen, W. Li, F. Zhang, X. Li, L. Xu, M. Sun, First-principle calculation of the electronic structures and optical properties of the metallic and nonmetallic elements-doped ZnO on the basis of photocatalysis. Physica B **555**, 53–60 (2019)
39. M. Kapilashrami, Y. Zhang, Y.-S. Liu, A. Hagfeldt, J. Guo, Probing the optical property and electronic structure of TiO_2 nanomaterials for renewable energy applications. Chem. Rev. **114**, 9662–9707 (2014)
40. S. Xu, E.A. Carter, Theoretical insights into heterogeneous (photo) electrochemical CO_2 reduction. Chem. Rev. **119**, 6631–6669 (2018)
41. H. Yang, F. Teng, W. Gu, Z. Liu, Y. Zhao, A. Zhang, Z. Liu, Y. Teng, A simple post-synthesis conversion approach to Zn (OH) F and the effects of fluorine and hydroxyl on the photodegradation properties of dye wastewater. J. Hazard. Mater. **333**, 250–258 (2017)
42. Z. Zhang, L. Wang, W. Liu, Z. Yan, Y. Zhu, S. Zhou, S. Guan, Photogenerated-hole-induced rapid elimination of solid tumors by the supramolecular porphyrin photocatalyst. Natl. Sci. Rev. **8**, naa155 (2021)
43. I. Okeke, C. Okeke, Molecular docking and analysis of in silico generated ligands against SARS-CoV-2 spike and replicase proteins (2022). https://doi.org/10.21203/rs.3.rs-2069911/v1.
44. C.O.L. Mbuya, C.G. Okoye-Chine, K. Ramutsindela, L.L. Jewell, M. Scurrell, Microwave modification of iron supported on beta silicon carbide catalysts for Fischer–Tropsch synthesis. React. Chem. Eng. **7**, 1307–1314 (2022)
45. R. Gandhi, A. Moses, S.S. Baral, Fundamental study of the photocatalytic reduction of CO_2: a short review of thermodynamics, kinetics and mechanisms. Chem. Process. Eng. **43**, 223–228 (2022)
46. T. Mavrič, *Synthesis and characterization of metal/semiconductor nanocomposites for photocatalysis* (Univerza v Novi Gorici, Fakulteta za podiplomski študij, 2017)
47. H. Liang, H. Zhang, P. Zhao, X. Zhao, H. Sun, Z. Geng, D. She, Synthesis of a novel three-dimensional porous carbon material and its highly selective Cr(VI) removal in wastewater. J. Clean. Prod. **306**, 127204 (2021)
48. J.R. Bolton, Solar fuels: the production of energy-rich compounds by the photochemical conversion and storage of solar energy. Science **202**, 705–711 (1978)
49. J.-M. Lehn, R. Ziessel, Photochemical generation of carbon monoxide and hydrogen by reduction of carbon dioxide and water under visible light irradiation. Proc. Natl. Acad. Sci. **79**, 701–704 (1982)
50. X. Tan, Y. Jiang, Y. Chen, A. Tong, J. Li, Y. Sun, Roles of different components of complex inclusion in pitting of 321 stainless steel: induction effect of CaS and inhibition effect of TiN. Corros. Sci. **209**, 110692 (2022)
51. G. Yasin, S. Ibraheem, S. Ali, M. Arif, S. Ibrahim, R. Iqbal, A. Kumar, M. Tabish, M. Mushtaq, A. Saad, Defects-engineered tailoring of tri-doped interlinked metal-free bifunctional catalyst with lower Gibbs free energy of OER/HER intermediates for overall water splitting. Mater. Today Chem. **23**, 100634 (2022)
52. X. Li, J. Yu, M. Jaroniec, X. Chen, Cocatalysts for selective photoreduction of CO_2 into solar fuels. Chem. Rev. **119**, 3962–4179 (2019)
53. K. Nakata, A. Fujishima, TiO2 photocatalysis: design and applications. J. Photochem. Photobiol. C **13**, 169–189 (2012)
54. A.L. Linsebigler, G. Lu, J.T. Yates Jr., Photocatalysis on TiO_2 surfaces: principles, mechanisms, and selected results. Chem. Rev. **95**, 735–758 (1995)
55. A. Dhakshinamoorthy, S. Navalon, A. Corma, H. Garcia, Photocatalytic CO_2 reduction by TiO_2 and related titanium containing solids. Energy Environ. Sci. **5**, 9217–9233 (2012)
56. V.P. Indrakanti, J.D. Kubicki, H.H. Schobert, Photoinduced activation of CO_2 on Ti-based heterogeneous catalysts: current state, chemical physics-based insights and outlook. Energy Environ. Sci. **2**, 745–758 (2009)
57. T. Inoue, A. Fujishima, S. Konishi, K. Honda, Photoelectrocatalytic reduction of carbon dioxide in aqueous suspensions of semiconductor powders. Nature **277**, 637–638 (1979)
58. J. Nunez, P. Jana, J.M. Coronado, D.P. Serrano, Effect of copper on the performance of ZnO and $ZnO_1{-}_xN_x$ oxides as CO_2 photoreduction catalysts. Catal. Today **209**, 21–27 (2013)
59. G. Xi, S. Ouyang, J. Ye, General synthesis of hybrid TiO_2 mesoporous "French fries" toward improved photocatalytic conversion of CO_2 into hydrocarbon fuel: a case of TiO_2/ZnO. Chem. A Eur. J. **17**, 9057–9061 (2011)
60. G. Guan, T. Kida, A. Yoshida, Reduction of carbon dioxide with water under concentrated sunlight using photocatalyst combined with Fe-based catalyst. Appl. Catal. B **41**, 387–396 (2003)
61. G. Mahmodi, S. Sharifnia, F. Rahimpour, S. Hosseini, Photocatalytic conversion of CO_2 and CH_4 using ZnO coated mesh: effect of operational parameters and optimization. Sol. Energy Mater. Sol. Cells **111**, 31–40 (2013)
62. H. Inoue, H. Moriwaki, K. Maeda, H. Yoneyama, Photoreduction of carbon dioxide using chalcogenide semiconductor microcrystals. J. Photochem. Photobiol. A **86**, 191–196 (1995)
63. H. Fujiwara, H. Hosokawa, K. Murakoshi, Y. Wada, S. Yanagida, Surface characteristics of ZnS nanocrystallites relating to their photocatalysis for CO_2 reduction1. Langmuir **14**, 5154–5159 (1998)

64. K. Kočí, M. Reli, O. Kozák, Z. Lacný, D. Plachá, P. Praus, L. Obalová, Influence of reactor geometry on the yield of CO_2 photocatalytic reduction. Catal. Today **176**, 212–214 (2011)
65. H. Zhou, J. Guo, P. Li, T. Fan, D. Zhang, J. Ye, Leaf-architectured 3D hierarchical artificial photosynthetic system of perovskite titanates towards CO_2 photoreduction into hydrocarbon fuels. Sci. Rep. **3**, 1667 (2013)
66. B. Aurian-Blajeni, M. Halmann, J. Manassen, Photoreduction of carbon dioxide and water into formaldehyde and methanol on semiconductor materials. Sol. Energy **25**, 165–170 (1980)
67. D. Sui, X. Yin, H. Dong, S. Qin, J. Chen, W. Jiang, Photocatalytically reducing CO_2 to methyl formate in methanol over Ag loaded $SrTiO_3$ nanocrystal catalysts. Catal. Lett. **142**, 1202–1210 (2012)
68. W.-H. Lee, C.-H. Liao, M.-F. Tsai, C.-W. Huang, J.C. Wu, A novel twin reactor for CO_2 photoreduction to mimic artificial photosynthesis. Appl. Catal. B **132**, 445–451 (2013)
69. S. Yamamura, H. Kojima, J. Iyoda, W. Kawai, Formation of ethyl alcohol in the photocatalytic reduction of carbon dioxide by SiC and ZnSe/metal powders. J. Electroanal. Chem. Interfacial Electrochem. **225**, 287–290 (1987)
70. H. Li, Y. Lei, Y. Huang, Y. Fang, Y. Xu, L. Zhu, X. Li, Photocatalytic reduction of carbon dioxide to methanol by Cu_2O/SiC nanocrystallite under visible light irradiation. J. Nat. Gas Chem. **20**, 145–150 (2011)
71. T.-C. Yang, F.-C. Chang, C.-Y. Peng, H.P. Wang, Y.-L. Wei, Photocatalytic reduction of CO_2 with SiC recovered from silicon sludge wastes. Environ. Technol. **36**, 2987–2990 (2015)
72. Y. Li, W.-N. Wang, Z. Zhan, M.-H. Woo, C.-Y. Wu, P. Biswas, Photocatalytic reduction of CO_2 with H_2O on mesoporous silica supported Cu/TiO_2 catalysts. Appl. Catal. B **100**, 386–392 (2010)
73. I.-H. Tseng, W.-C. Chang, J.C. Wu, Photoreduction of CO_2 using sol–gel derived titania and titania-supported copper catalysts. Appl. Catal. B **37**, 37–48 (2002)
74. Y. Bessekhouad, D. Robert, J.-V. Weber, Photocatalytic activity of Cu_2O/TiO_2, Bi_2O_3/TiO_2 and $ZnMn_2O_4/TiO_2$ heterojunctions. Catal. Today **101**, 315–321 (2005)
75. D. Robert, Photosensitization of TiO_2 by MxOy and MxSy nanoparticles for heterogeneous photocatalysis applications. Catal. Today **122**, 20–26 (2007)
76. H. Fujiwara, H. Hosokawa, K. Murakoshi, Y. Wada, S. Yanagida, T. Okada, H. Kobayashi, Effect of surface structures on photocatalytic CO_2 reduction using quantized CdS nanocrystallites. J. Phys. Chem. B **101**, 8270–8278 (1997)
77. B.-J. Liu, T. Torimoto, H. Yoneyama, Photocatalytic reduction of CO_2 using surface-modified CdS photocatalysts in organic solvents. J. Photochem. Photobiol. A **113**, 93–97 (1998)
78. X. Li, J. Chen, H. Li, J. Li, Y. Xu, Y. Liu, J. Zhou, Photoreduction of CO_2 to methanol over Bi_2S_3/CdS photocatalyst under visible light irradiation. J. Nat. Gas Chem. **20**, 413–417 (2011)
79. P. Praus, O. Kozák, K. Kočí, A. Panáček, R. Dvorský, CdS nanoparticles deposited on montmorillonite: preparation, characterization and application for photoreduction of carbon dioxide. J. Colloid Interface Sci. **360**, 574–579 (2011)
80. Y.S. Chaudhary, T.W. Woolerton, C.S. Allen, J.H. Warner, E. Pierce, S.W. Ragsdale, F.A. Armstrong, Visible light-driven CO_2 reduction by enzyme coupled CdS nanocrystals. Chem. Commun. **48**, 58–60 (2012)
81. X. Li, H. Liu, D. Luo, J. Li, Y. Huang, H. Li, Y. Fang, Y. Xu, L. Zhu, Adsorption of CO_2 on heterostructure CdS (Bi_2S_3)/TiO_2 nanotube photocatalysts and their photocatalytic activities in the reduction of CO_2 to methanol under visible light irradiation. Chem. Eng. J. **180**, 151–158 (2012)
82. E.E. Barton, D.M. Rampulla, A.B. Bocarsly, Selective solar-driven reduction of CO_2 to methanol using a catalyzed p-GaP based photoelectrochemical cell. J. Am. Chem. Soc. **130**, 6342–6344 (2008)
83. K. Sekizawa, K. Maeda, K. Domen, K. Koike, O. Ishitani, Artificial Z-scheme constructed with a supramolecular metal complex and semiconductor for the photocatalytic reduction of CO_2. J. Am. Chem. Soc. **135**, 4596–4599 (2013)
84. M. Hara, J. Nunoshige, T. Takata, J.N. Kondo, K. Domen, Unusual enhancement of H_2 evolution by Ru on TaON photocatalyst under visible light irradiation. Chem. Commun. **2003**, 3000–3001 (2003)
85. E.S. Kim, N. Nishimura, G. Magesh, J.Y. Kim, J.-W. Jang, H. Jun, J. Kubota, K. Domen, J.S. Lee, Fabrication of $CaFe_2O_4$/TaON heterojunction photoanode for photoelectrochemical water oxidation. J. Am. Chem. Soc. **135**, 5375–5383 (2013)
86. K. Maeda, M. Higashi, D. Lu, R. Abe, K. Domen, Efficient nonsacrificial water splitting through two-step photoexcitation by visible light using a modified oxynitride as a hydrogen evolution photocatalyst. J. Am. Chem. Soc. **132**, 5858–5868 (2010)
87. J. Mao, T. Peng, X. Zhang, K. Li, L. Ye, L. Zan, Effect of graphitic carbon nitride microstructures on the activity and selectivity of photocatalytic CO_2 reduction under visible light. Catal. Sci. Technol. **3**, 1253–1260 (2013)
88. J. Yu, S. Wang, B. Cheng, Z. Lin, F. Huang, Noble metal-free Ni (OH) 2–gC_3N_4 composite photocatalyst with enhanced visible-light photocatalytic H_2-production activity. Catal. Sci. Technol. **3**, 1782–1789 (2013)
89. J. Zhang, X. Chen, K. Takanabe, K. Maeda, K. Domen, J.D. Epping, X. Fu, M. Antonietti, X. Wang, Synthesis of a carbon nitride structure for visible-light catalysis by copolymerization. Angew. Chem. Int. Ed. **49**, 441–444 (2010)
90. A. Kudo, K. Ueda, H. Kato, I. Mikami, Photocatalytic O_2 evolution under visible light irradiation on $BiVO_4$ in aqueous $AgNO_3$ solution. Catal. Lett. **53**, 229–230 (1998)
91. A. Kudo, K. Omori, H. Kato, A novel aqueous process for preparation of crystal form-controlled and highly crystalline $BiVO_4$ powder from layered vanadates at room temperature and its photocatalytic and photophysical properties. J. Am. Chem. Soc. **121**, 11459–11467 (1999)
92. S. Tokunaga, H. Kato, A. Kudo, Selective preparation of monoclinic and tetragonal $BiVO_4$ with scheelite structure and their photocatalytic properties. Chem. Mater. **13**, 4624–4628 (2001)
93. H. Jiang, H. Dai, X. Meng, K. Ji, L. Zhang, J. Deng, Porous olive-like $BiVO_4$: alcoho-hydrothermal preparation and excellent visible-light-driven photocatalytic performance for the degradation of phenol. Appl. Catal. B **105**, 326–334 (2011)
94. H. Jiang, X. Meng, H. Dai, J. Deng, Y. Liu, L. Zhang, Z. Zhao, R. Zhang, High-performance porous spherical or octapod-like single-crystalline $BiVO_4$ photocatalysts for the removal of phenol and methylene blue under visible-light illumination. J. Hazard. Mater. **217**, 92–99 (2012)
95. W.-J. Chun, A. Ishikawa, H. Fujisawa, T. Takata, J.N. Kondo, M. Hara, M. Kawai, Y. Matsumoto, K. Domen, Conduction and valence band positions of Ta_2O_5, TaON, and Ta_3N_5 by UPS and electrochemical methods. J. Phys. Chem. B **107**, 1798–1803 (2003)
96. M. Higashi, K. Domen, R. Abe, Fabrication of efficient TaON and Ta_3N_5 photoanodes for water splitting under visible light irradiation. Energy Environ. Sci. **4**, 4138–4147 (2011)
97. Y. Li, T. Takata, D. Cha, K. Takanabe, T. Minegishi, J. Kubota, K. Domen, Vertically aligned Ta3N5 nanorod arrays for solar-driven photoelectrochemical water splitting. Adv. Mater. **25**, 125–131 (2013)
98. S.S.K. Ma, T. Hisatomi, K. Maeda, Y. Moriya, K. Domen, Enhanced water oxidation on Ta3N5 photocatalysts by

modification with alkaline metal salts. J. Am. Chem. Soc. **134**, 19993–19996 (2012)
99. X. Yang, C. Cao, L. Erickson, K. Hohn, R. Maghirang, K. Klabunde, Synthesis of visible-light-active TiO_2-based photocatalysts by carbon and nitrogen doping. J. Catal. **260**, 128–133 (2008)
100. D. Jiang, Y. Xu, D. Wu, Y. Sun, Isocyanate-modified TiO_2 visible-light-activated photocatalyst. Appl. Catal. B **88**, 165–172 (2009)
101. K. Villa, A. Black, X. Domenech, J. Peral, Nitrogen doped TiO_2 for hydrogen production under visible light irradiation. Sol. Energy **86**, 558–566 (2012)
102. S. Qin, S.L. Chan, S. Gu, Y. Bai, Z. Ren, X. Lin, Z. Chen, W. Jia, Y. Jin, Y. Guo, Camrelizumab plus rivoceranib versus sorafenib as first-line therapy for unresectable hepatocellular carcinoma (CARES-310): a randomised, open-label, international phase 3 study. The Lancet **402**, 1133–1146 (2023)
103. Y. Zou, S. Wang, An investigation of active sites for electrochemical CO_2 reduction reactions: from in situ characterization to rational design. Adv. Sci. **8**, 2003579 (2021)
104. M. Dunwell, W. Luc, Y. Yan, F. Jiao, B. Xu, Understanding surface-mediated electrochemical reactions: CO_2 reduction and beyond. ACS Catal. **8**, 8121–8129 (2018)
105. A.J. Morris, G.J. Meyer, E. Fujita, Molecular approaches to the photocatalytic reduction of carbon dioxide for solar fuels. Acc. Chem. Res. **42**, 1983–1994 (2009)
106. Z. Yu, K. Zheng, X. Li, P. Xia, J. Xu, J. Sun, N. Zhou, F. Pan, Effect of Ti6Al4V reinforcement particles on the mechanical, wear, and corrosion properties of AZ91D magnesium matrix composites. J. Market. Res. **26**, 7395–7411 (2023)
107. I. Willner, R. Maidan, D. Mandler, H. Duerr, G. Doerr, K. Zengerle, Photosensitized reduction of carbon dioxide to methane and hydrogen evolution in the presence of ruthenium and osmium colloids: strategies to design selectivity of products distribution. J. Am. Chem. Soc. **109**, 6080–6086 (1987)
108. A. Yahaya, M. Gondal, A. Hameed, Selective laser enhanced photocatalytic conversion of CO_2 into methanol. Chem. Phys. Lett. **400**, 206–212 (2004)
109. W.A. Thompson, E. Sanchez Fernandez, M.M. Maroto-Valer, Review and analysis of CO_2 photoreduction kinetics. ACS Sustain. Chem. Eng. **8**, 4677–4692 (2020)
110. M. Tahir, N.S. Amin, Photocatalytic CO_2 reduction with H_2O vapors using montmorillonite/TiO_2 supported microchannel monolith photoreactor. Chem. Eng. J. **230**, 314–327 (2013)
111. L.-L. Tan, W.-J. Ong, S.-P. Chai, A.R. Mohamed, Photocatalytic reduction of CO_2 with H_2O over graphene oxide-supported oxygen-rich TiO_2 hybrid photocatalyst under visible light irradiation: process and kinetic studies. Chem. Eng. J. **308**, 248–255 (2017)
112. A. Khalilzadeh, A. Shariati, Photoreduction of CO_2 over heterogeneous modified TiO_2 nanoparticles under visible light irradiation: synthesis, process and kinetic study. Sol. Energy **164**, 251–261 (2018)
113. S. Delavari, N.A.S. Amin, Photocatalytic conversion of CO_2 and CH4 over immobilized titania nanoparticles coated on mesh: optimization and kinetic study. Appl. Energy **162**, 1171–1185 (2016)
114. M. Tahir, N.S. Amin, Indium-doped TiO_2 nanoparticles for photocatalytic CO_2 reduction with H_2O vapors to CH_4. Appl. Catal. B **162**, 98–109 (2015)
115. J.C. Wu, H.-M. Lin, C.-L. Lai, Photo reduction of CO_2 to methanol using optical-fiber photoreactor. Appl. Catal. A **296**, 194–200 (2005)
116. Y. Ku, W.-H. Lee, W.-Y. Wang, Photocatalytic reduction of carbonate in aqueous solution by UV/TiO_2 process. J. Mol. Catal. A: Chem. **212**, 191–196 (2004)
117. S. Jain, G. Dangi, J. Vardia, S.C. Ameta, Photocatalytic reduction of some alkali carbonates in the presence of methylene blue. Int. J. Energy Res. **23**, 71–77 (1999)
118. J. Ran, M. Jaroniec, S.Z. Qiao, Cocatalysts in semiconductor-based photocatalytic CO_2 reduction: achievements, challenges, and opportunities. Adv. Mater. **30**, 1704649 (2018)
119. J. Ângelo, L. Andrade, L.M. Madeira, A. Mendes, An overview of photocatalysis phenomena applied to NO_x abatement. J. Environ. Manag. **129**, 522–539 (2013)
120. H. Chen, C.E. Nanayakkara, V.H. Grassian, Titanium dioxide photocatalysis in atmospheric chemistry. Chem. Rev. **112**, 5919–5948 (2012)
121. S. Nahar, M. Zain, A.A.H. Kadhum, H.A. Hasan, M.R. Hasan, Advances in photocatalytic CO_2 reduction with water: a review. Materials **10**, 629 (2017)
122. J.M. Luo, C.F. Lam, Travel anxiety, risk attitude and travel intentions towards "travel bubble" destinations in Hong Kong: effect of the fear of COVID-19. Int. J. Environ. Res. Public Health **17**, 7859 (2020)
123. M. Cheng, P. He, L. Lei, X. Tan, X. Wang, Y. Sun, J. Li, Y. Jiang, Comparative studies on microstructure evolution and corrosion resistance of 304 and a newly developed high Mn and N austenitic stainless steel welded joints. Corros. Sci. **183**, 109338 (2021)
124. W. Fan, Q. Zhang, Y. Wang, Semiconductor-based nanocomposites for photocatalytic H_2 production and CO_2 conversion. Phys. Chem. Chem. Phys. **15**, 2632–2649 (2013)
125. S. Shen, J. Shi, P. Guo, L. Guo, Visible-light-driven photocatalytic water splitting on nanostructured semiconducting materials. Int. J. Nanotechnol. **8**, 523–591 (2011)
126. P. Rajesh, F.H. Shajin, B.N. Kommula, An efficient integration and control approach to increase the conversion efficiency of high-current low-voltage DC/DC converter. Energy Syst. **13**, 939–958 (2022)
127. J. Yu, J. Jin, B. Cheng, M. Jaroniec, A noble metal-free reduced graphene oxide–CdS nanorod composite for the enhanced visible-light photocatalytic reduction of CO_2 to solar fuel. J. Mater. Chem. A **2**, 3407–3416 (2014)
128. J. Lin, Z. Pan, X. Wang, Photochemical reduction of CO_2 by graphitic carbon nitride polymers. ACS Sustain. Chem. Eng. **2**, 353–358 (2014)
129. J. Yu, K. Wang, W. Xiao, B. Cheng, Photocatalytic reduction of CO_2 into hydrocarbon solar fuels over gC_3N_4–Pt nanocomposite photocatalysts. Phys. Chem. Chem. Phys. **16**, 11492–11501 (2014)
130. Y. Liu, Z. Wang, B. Huang, Y. Dai, X. Qin, X. Zhang, Microstructure modulation of semiconductor photocatalysts for CO_2 reduction. Curr. Org. Chem. **18**, 620–628 (2014)
131. Y.P. Xie, G. Liu, L. Yin, H.-M. Cheng, Crystal facet-dependent photocatalytic oxidation and reduction reactivity of monoclinic WO_3 for solar energy conversion. J. Mater. Chem. **22**, 6746–6751 (2012)
132. Y. Matsumoto, Energy positions of oxide semiconductors and photocatalysis with iron complex oxides. J. Solid State Chem. **126**, 227–234 (1996)
133. L. Jia, J. Li, W. Fang, Enhanced visible-light active C and Fe co-doped $LaCoO_3$ for reduction of carbon dioxide. Catal. Commun. **11**, 87–90 (2009)
134. Y. Liu, B. Huang, Y. Dai, X. Zhang, X. Qin, M. Jiang, M.-H. Whangbo, Selective ethanol formation from photocatalytic reduction of carbon dioxide in water with $BiVO_4$ photocatalyst. Catal. Commun. **11**, 210–213 (2009)
135. J. Mao, T. Peng, X. Zhang, K. Li, L. Zan, Selective methanol production from photocatalytic reduction of CO_2 on $BiVO_4$ under visible light irradiation. Catal. Commun. **28**, 38–41 (2012)
136. Y. Zhou, Z. Tian, Z. Zhao, Q. Liu, J. Kou, X. Chen, J. Gao, S. Yan, Z. Zou, High-yield synthesis of ultrathin and uniform Bi_2WO_6

square nanoplates benefitting from photocatalytic reduction of CO_2 into renewable hydrocarbon fuel under visible light. ACS Appl. Mater. Interfaces **3**, 3594–3601 (2011)
137. H. Cheng, B. Huang, Y. Liu, Z. Wang, X. Qin, X. Zhang, Y. Dai, An anion exchange approach to Bi_2 WO_6 hollow microspheres with efficient visible light photocatalytic reduction of CO_2 to methanol. Chem. Commun. **48**, 9729–9731 (2012)
138. P. Li, Y. Zhou, W. Tu, Q. Liu, S. Yan, Z. Zou, Direct growth of $Fe_2V_4O_{13}$ nanoribbons on a stainless-steel mesh for visible-light photoreduction of CO_2 into renewable hydrocarbon fuel and degradation of gaseous isopropyl alcohol. ChemPlusChem **78**, 274–278 (2013)
139. Z.-Y. Wang, H.-C. Chou, J.C. Wu, D.P. Tsai, G. Mul, CO_2 photoreduction using $NiO/InTaO_4$ in optical-fiber reactor for renewable energy. Appl. Catal. A **380**, 172–177 (2010)
140. P.-W. Pan, Y.-W. Chen, Photocatalytic reduction of carbon dioxide on $NiO/InTaO_4$ under visible light irradiation. Catal. Commun. **8**, 1546–1549 (2007)
141. H.-C. Chen, H.-C. Chou, J.C. Wu, H.-Y. Lin, Sol–gel prepared $InTaO_4$ and its photocatalytic characteristics. J. Mater. Res. **23**, 1364–1370 (2008)
142. C.-W. Tsai, H.M. Chen, R.-S. Liu, K. Asakura, T.-S. Chan, Ni@NiO core–shell structure-modified nitrogen-doped $InTaO_4$ for solar-driven highly efficient CO_2 reduction to methanol. J. Phys. Chem. C **115**, 10180–10186 (2011)
143. W. Shi, M. Laabs, M. Reinmoeller, L. Kong, S.V. Vassilev, S. Guhl, J. Bai, B. Meyer, W. Li, The fusion mechanism of complex minerals mixture and prediction model for flow temperature of coal ash for gasification. Fuel **305**, 121448 (2021)
144. S. Li, Y. Wu, H. Zheng, H. Li, Y. Zheng, J. Nan, J. Ma, D. Nagarajan, J.-S. Chang, Antibiotics degradation by advanced oxidation process (AOPs): recent advances in ecotoxicity and antibiotic-resistance genes induction of degradation products. Chemosphere **311**, 136977 (2023)
145. N. Serpone, A. Emeline, *Semiconductor Photocatalysis—Past, Present, and Future Outlook* (ACS Publications, London, 2012), pp.673–677
146. J.-X. Wang, Y. Zhao, M.-S. Chen, H. Zhang, J.-G. Cui, J.-L. Li, Heme-oxygenase-1 as a target for phthalate-induced cardiomyocytes ferroptosis. Environ. Pollut. **317**, 120717 (2023)
147. L.G. Devi, R. Kavitha, A review on non metal ion doped titania for the photocatalytic degradation of organic pollutants under UV/solar light: role of photogenerated charge carrier dynamics in enhancing the activity. Appl. Catal. B **140**, 559–587 (2013)
148. R. Huang, J. Wu, M. Zhang, B. Liu, Z. Zheng, D. Luo, Strategies to enhance photocatalytic activity of graphite carbon nitride-based photocatalysts. Mater. Des. **210**, 110040 (2021)
149. F.A. Qaraah, S.A. Mahyoub, Q.A. Drmosh, A. Qaraah, F. Xin, One-step fabrication of unique 3D/2D S, O-doped g-C3N4 S-scheme isotype heterojunction for boosting CO_2 photoreduction. Mater. Today Sustain. **23**, 100437 (2023)
150. N. Serpone, *Is the Band Gap of Pristine TiO_2 Narrowed by Anion-and Cation-Doping of Titanium Dioxide in Second-Generation Photocatalysts?* (ACS Publications, London, 2006), pp. 24287–24293.
151. S.B. Patil, P.S. Basavarajappa, N. Ganganagappa, M. Jyothi, A. Raghu, K.R. Reddy, Recent advances in non-metals-doped TiO_2 nanostructured photocatalysts for visible-light driven hydrogen production, CO_2 reduction and air purification. Int. J. Hydrog. Energy **44**, 13022–13039 (2019)
152. N. Shehzad, M. Tahir, K. Johari, T. Murugesan, M. Hussain, A critical review on TiO_2 based photocatalytic CO_2 reduction system: strategies to improve efficiency. J. CO_2 Util. **26**, 98–122 (2018).
153. Y. Yan, Y. Yu, S. Huang, Y. Yang, X. Yang, S. Yin, Y. Cao, Adjustment and matching of energy band of TiO_2-based photocatalysts by metal ions (Pd, Cu, Mn) for photoreduction of CO_2 into CH_4. J. Phys. Chem. C **121**, 1089–1098 (2017)
154. Y. Sohn, W. Huang, F. Taghipour, Recent progress and perspectives in the photocatalytic CO_2 reduction of Ti-oxide-based nanomaterials. Appl. Surf. Sci. **396**, 1696–1711 (2017)
155. J. Jiao, Y. Wei, K. Chi, Z. Zhao, A. Duan, J. Liu, G. Jiang, Y. Wang, X. Wang, C. Han, Platinum nanoparticles supported on TiO_2 photonic crystals as highly active photocatalyst for the reduction of CO_2 in the presence of water. Energ. Technol. **5**, 877–883 (2017)
156. M. Tahir, B. Tahir, N.A.S. Amin, H. Alias, Selective photocatalytic reduction of CO_2 by H_2O/H_2 to CH_4 and CH_3OH over Cu-promoted In_2O_3/TiO_2 nanocatalyst. Appl. Surf. Sci. **389**, 46–55 (2016)
157. B. Yu, Y. Zhou, P. Li, W. Tu, P. Li, L. Tang, J. Ye, Z. Zou, Photocatalytic reduction of CO_2 over Ag/TiO_2 nanocomposites prepared with a simple and rapid silver mirror method. Nanoscale **8**, 11870–11874 (2016)
158. M. Tahir, B. Tahir, N.A.S. Amin, A. Muhammad, Photocatalytic CO_2 methanation over NiO/In_2O_3 promoted TiO_2 nanocatalysts using H_2O and/or H_2 reductants. Energy Convers. Manag. **119**, 368–378 (2016)
159. X. Meng, S. Ouyang, T. Kako, P. Li, Q. Yu, T. Wang, J. Ye, Photocatalytic CO_2 conversion over alkali modified TiO_2 without loading noble metal cocatalyst. Chem. Commun. **50**, 11517–11519 (2014)
160. L. Collado, A. Reynal, J. Coronado, D. Serrano, J. Durrant, V. De la Peña O'Shea, Effect of Au surface plasmon nanoparticles on the selective CO_2 photoreduction to CH4. Appl. Catal. B Environ. **178**, 177–185 (2015).
161. Y. Kohno, H. Hayashi, S. Takenaka, T. Tanaka, T. Funabiki, S. Yoshida, Photo-enhanced reduction of carbon dioxide with hydrogen over Rh/TiO_2. J. Photochem. Photobiol. A **126**, 117–123 (1999)
162. Y.T. Liang, B.K. Vijayan, O. Lyandres, K.A. Gray, M.C. Hersam, Effect of dimensionality on the photocatalytic behavior of carbon–titania nanosheet composites: charge transfer at nanomaterial interfaces. J. Phys. Chem. Lett. **3**, 1760–1765 (2012)
163. J.F. de Brito, M.V.B. Zanoni, On the application of $Ti/TiO_2/CuO$ np junction semiconductor: a case study of electrolyte, temperature and potential influence on CO_2 reduction. Chem. Eng. J. **318**, 264–271 (2017)
164. J. Fan, E.-Z. Liu, L. Tian, X.-Y. Hu, Q. He, T. Sun, Synergistic effect of N and Ni^{2+} on nanotitania in photocatalytic reduction of CO_2. J. Environ. Eng. **137**, 171–176 (2011)
165. A. Sharma, B.-K. Lee, Photocatalytic reduction of carbon dioxide to methanol using nickel-loaded TiO_2 supported on activated carbon fiber. Catal. Today **298**, 158–167 (2017)
166. X. Li, Q. Wang, Y. Zhao, W. Wu, J. Chen, H. Meng, Green synthesis and photo-catalytic performances for ZnO-reduced graphene oxide nanocomposites. J. Colloid Interface Sci. **411**, 69–75 (2013)
167. Q. Zhang, C.-F. Lin, Y.H. Jing, C.-T. Chang, Photocatalytic reduction of carbon dioxide to methanol and formic acid by graphene-TiO_2. J. Air Waste Manag. Assoc. **64**, 578–585 (2014)
168. K. Thamaraiselvi, T. Sivakumar, Photocatalytic reduction of carbon dioxide by using bare and copper oxide impregnated nano titania catalysts. J. Nanosci. Nanotechnol. **17**, 313–322 (2017)
169. T. Zhang, J. Low, X. Huang, J.F. Al-Sharab, J. Yu, T. Asefa, Copper-decorated microsized nanoporous titanium dioxide photocatalysts for carbon dioxide reduction by water. ChemCatChem **9**, 3054–3062 (2017)
170. G. Xi, S. Ouyang, P. Li, J. Ye, Q. Ma, N. Su, H. Bai, C. Wang, Ultrathin W18O49 nanowires with diameters below 1 nm: synthesis, near-infrared absorption, photoluminescence, and

photochemical reduction of carbon dioxide. Angew. Chem. Int. Ed. **51**, 2395–2399 (2012)
171. X. Pan, M.-Q. Yang, X. Fu, N. Zhang, Y.-J. Xu, Defective TiO_2 with oxygen vacancies: synthesis, properties and photocatalytic applications. Nanoscale **5**, 3601–3614 (2013)
172. M. Huang, T. Tang, P. Pang, M. Li, R. Ma, J. Lu, J. Shu, Y. You, B. Chen, J. Liang, Treating COVID-19 with chloroquine. J. Mol. Cell Biol. **12**, 322–325 (2020)
173. L. Liu, H. Zhao, J.M. Andino, Y. Li, Photocatalytic CO_2 reduction with H_2O on TiO_2 nanocrystals: comparison of anatase, rutile, and brookite polymorphs and exploration of surface chemistry. ACS Catal. **2**, 1817–1828 (2012)
174. D.R. Eddy, M.D. Permana, L.K. Sakti, G.A.N. Sheha, Solihudin, S. Hidayat, T. Takei, N. Kumada, I. Rahayu, Heterophase polymorph of TiO_2 (Anatase, Rutile, Brookite, TiO_2 (B)) for efficient photocatalyst: fabrication and activity. Nanomaterials **13** (2023) 704.
175. G. Tompsett, G. Bowmaker, R. Cooney, J. Metson, K. Rodgers, J. Seakins, The Raman spectrum of brookite, TiO_2 (PBCA, Z = 8). J. Raman Spectrosc. **26**, 57–62 (1995)
176. A. Beltran, L. Gracia, J. Andres, Density functional theory study of the brookite surfaces and phase transitions between natural titania polymorphs. J. Phys. Chem. B **110**, 23417–23423 (2006)
177. Z. Li, S. Cong, Y. Xu, Brookite vs anatase TiO_2 in the photocatalytic activity for organic degradation in water. ACS Catal. **4**, 3273–3280 (2014)
178. Z. Zhang, Y. Li, J. Shi, L. Zhu, Y. Dai, P. Fu, S. Liu, M. Hong, J. Zhang, J. Wang, Lymphocyte-related immunomodulatory therapy with siponimod (BAF-312) improves outcomes in mice with acute intracerebral hemorrhage. Aging Dis. **14**, 966 (2023)
179. B.A. Malla, S. Ramanjeneya, J. Vergis, S.S. Malik, S.B. Barbuddhe, D.B. Rawool, Comparison of recombinant and synthetic listeriolysin-O peptide-based indirect ELISA vis-à-vis cultural isolation for detection of listeriosis in caprine and ovine species. J. Microbiol. Methods **188**, 106278 (2021)
180. A.S. Malik, H. Bali, F. Czirok, Á. Szamosvölgyi, G. Halasi, A. Efremova, B. Šmíd, A. Sápi, Á. Kukovecz, Z. Kónya, Turning CO_2 to CH4 and CO over CeO_2 and MCF-17 supported Pt, Ru and Rh nanoclusters—influence of nanostructure morphology, supporting materials and operating conditions. Fuel **326**, 124994 (2022)
181. F. Bibi, M.I. Ali, M. Ahmad, A. Bokhari, K.S. Khoo, M. Zafar, S. Asif, M. Mubashir, N. Han, P.L. Show, Production of lipids biosynthesis from *Tetradesmus nygaardii* microalgae as a feedstock for biodiesel production. Fuel **326**, 124985 (2022)
182. K.S. Novoselov, A.K. Geim, S.V. Morozov, D.-E. Jiang, Y. Zhang, S.V. Dubonos, I.V. Grigorieva, A.A. Firsov, Electric field effect in atomically thin carbon films. Science **306**, 666–669 (2004)
183. A.K. Geim, K.S. Novoselov, The rise of graphene. Nat. Mater. **6**, 183–191 (2007)
184. K. Thodkar, F. Gramm, Enhanced mobility in suspended chemical vapor-deposited graphene field-effect devices in ambient conditions. ACS Appl. Mater. Interfaces **15**, 37756–37763 (2023)
185. C. Shu, H.-Y. Zhao, S. Zhao, W. Deng, P. Min, X.-H. Lu, X. Li, Z.-Z. Yu, Highly thermally conductive phase change composites with anisotropic graphene/cellulose nanofiber hybrid aerogels for efficient temperature regulation and solar-thermal-electric energy conversion applications. Compos. B Eng. **248**, 110367 (2023)
186. A.R. Urade, I. Lahiri, K. Suresh, Graphene properties, synthesis and applications: a review. JOM **75**, 614–630 (2023)
187. R. Wazalwar, M. Sahu, *Novel Applications of Graphene in the Aerospace Industry, Novel Applications of Carbon Based Nano-Materials* (CRC Press, Boca Raton, 2022), pp.180–198
188. A. Armano, S. Agnello, Two-dimensional carbon: a review of synthesis methods, and electronic, optical, and vibrational properties of single-layer graphene. C **5**, 67 (2019)
189. S. Chakraborty, R. Saha, S. Saha, A critical review on graphene and graphene-based derivatives from natural sources emphasizing on CO_2 adsorption potential. Environ. Sci. Pollut. Res. **2023**, 1–31 (2023)
190. S.-Y. Lee, S.-J. Park, A review on solid adsorbents for carbon dioxide capture. J. Ind. Eng. Chem. **23**, 1–11 (2015)
191. N.A.F. Mazri, A. Arifutzzaman, M.K. Aroua, M.E. Rahman, S.A. Mazari, Graphene and its tailoring as emerging 2D nanomaterials in efficient CO_2 absorption: a state-of-the-art interpretative review. Alex. Eng. J. **77**, 479–502 (2023)
192. A. Ghosh, K. Subrahmanyam, K.S. Krishna, S. Datta, A. Govindaraj, S.K. Pati, C. Rao, Uptake of H_2 and CO_2 by graphene. J. Phys. Chem. C **112**, 15704–15707 (2008)
193. L. Ekhlasi, H. Younesi, A. Rashidi, N. Bahramifar, Populus wood biomass-derived graphene for high CO_2 capture at atmospheric pressure and estimated cost of production. Process. Saf. Environ. Prot. **113**, 97–108 (2018)
194. M.O. Aquatar, J.S. Mankar, U. Bhatia, S.S. Rayalu, R.J. Krupadam, Graphene nanosheets from hazardous/solid wastes: an efficient CO_2 capture material. J. Environ. Chem. Eng. **9**, 105839 (2021)
195. S. Chowdhury, R. Balasubramanian, Highly efficient, rapid and selective CO_2 capture by thermally treated graphene nanosheets. J. CO_2 Util. **13** (2016) 50–60.
196. L.-Y. Meng, S.-J. Park, Effect of exfoliation temperature on carbon dioxide capture of graphene nanoplates. J. Colloid Interface Sci. **386**, 285–290 (2012)
197. J. Pokhrel, N. Bhoria, S. Anastasiou, T. Tsoufis, D. Gournis, G. Romanos, G.N. Karanikolos, CO_2 adsorption behavior of amine-functionalized ZIF-8, graphene oxide, and ZIF-8/graphene oxide composites under dry and wet conditions. Microporous Mesoporous Mater. **267**, 53–67 (2018)
198. N. Politakos, I. Barbarin, L.S. Cantador, J.A. Cecilia, E. Mehravar, R. Tomovska, Graphene-based monolithic nanostructures for CO_2 capture. Ind. Eng. Chem. Res. **59**, 8612–8621 (2020)
199. M. Aggarwal, S. Basu, N.P. Shetti, M.N. Nadagouda, T.M. Aminabhavi, Photocatalytic conversion of CO_2 into valuable products using emerging two-dimensional graphene-based nanomaterials: a step towards sustainability. Chem. Eng. J. **425**, 131401 (2021)
200. Y. Kuang, J. Shang, T. Zhu, Photoactivated graphene oxide to enhance photocatalytic reduction of CO_2. ACS Appl. Mater. Interfaces **12**, 3580–3591 (2019)
201. X. Wang, K. Li, J. He, J. Yang, F. Dong, W. Mai, M. Zhu, Defect in reduced graphene oxide tailored selectivity of photocatalytic CO_2 reduction on Cs4PbBr 6 pervoskite hole-in-microdisk structure. Nano Energy **78**, 105388 (2020)
202. P. Devi, J. Singh, Visible light induced selective photocatalytic reduction of CO_2 to CH_4 on In_2O_3-rGO nanocomposites. J. CO_2 Util. **43** (2021) 101376.
203. L.-Y. Lin, Y. Nie, S. Kavadiya, T. Soundappan, P. Biswas, N-doped reduced graphene oxide promoted nano TiO_2 as a bifunctional adsorbent/photocatalyst for CO_2 photoreduction: Effect of N species. Chem. Eng. J. **316**, 449–460 (2017)
204. C. Bie, B. Zhu, F. Xu, L. Zhang, J. Yu, In situ grown monolayer N-doped graphene on CdS hollow spheres with seamless contact for photocatalytic CO_2 reduction. Adv. Mater. **31**, 1902868 (2019)
205. C.B. Hiragond, J. Lee, H. Kim, J.-W. Jung, C.-H. Cho, S.-I. In, A novel N-doped graphene oxide enfolded reduced titania for highly stable and selective gas-phase photocatalytic CO_2 reduction into CH4: an in-depth study on the interfacial charge transfer mechanism. Chem. Eng. J. **416**, 127978 (2021)

206. M.R.U.D. Biswas, A. Ali, K.Y. Cho, W.-C. Oh, Novel synthesis of WSe_2-graphene-TiO_2 ternary nanocomposite via ultrasonic technics for high photocatalytic reduction of CO_2 into CH3OH. Ultrason. Sonochem. **42**, 738–746 (2018)
207. L. Zhang, N. Li, H. Jiu, G. Qi, Y. Huang, ZnO-reduced graphene oxide nanocomposites as efficient photocatalysts for photocatalytic reduction of CO_2. Ceram. Int. **41**, 6256–6262 (2015)
208. J.O. Olowoyo, M. Kumar, B. Singh, V.O. Oninla, J.O. Babalola, H. Valdés, A.V. Vorontsov, U. Kumar, Self-assembled reduced graphene oxide-TiO_2 nanocomposites: synthesis, DFTB+ calculations, and enhanced photocatalytic reduction of CO_2 to methanol. Carbon **147**, 385–397 (2019)
209. W.-J. Ong, L.-L. Tan, S.-P. Chai, S.-T. Yong, Graphene oxide as a structure-directing agent for the two-dimensional interface engineering of sandwich-like graphene–gC_3N_4 hybrid nanostructures with enhanced visible-light photoreduction of CO_2 to methane. Chem. Commun. **51**, 858–861 (2015)
210. Z. Tong, D. Yang, J. Shi, Y. Nan, Y. Sun, Z. Jiang, Three-dimensional porous aerogel constructed by g-C_3N_4 and graphene oxide nanosheets with excellent visible-light photocatalytic performance. ACS Appl. Mater. Interfaces **7**, 25693–25701 (2015)
211. W.-J. Ong, L.-L. Tan, S.-P. Chai, S.-T. Yong, A.R. Mohamed, Surface charge modification via protonation of graphitic carbon nitride (g-C_3N_4) for electrostatic self-assembly construction of 2D/2D reduced graphene oxide (rGO)/g-C_3N_4 nanostructures toward enhanced photocatalytic reduction of carbon dioxide to methane. Nano Energy **13**, 757–770 (2015)
212. C. Han, Y. Lei, B. Wang, Y. Wang, In situ-fabricated 2D/2D heterojunctions of ultrathin SiC/reduced graphene oxide nanosheets for efficient CO_2 photoreduction with high CH_4 selectivity. Chemsuschem **11**, 4237–4245 (2018)
213. A. Bafaqeer, M. Tahir, N.A.S. Amin, Synergistic effects of 2D/2D ZnV2O6/RGO nanosheets heterojunction for stable and high performance photo-induced CO_2 reduction to solar fuels. Chem. Eng. J. **334**, 2142–2153 (2018)
214. Z. Otgonbayar, K.Y. Cho, W.-C. Oh, Enhanced photocatalytic activity of CO_2 reduction to methanol through the use of a novel-structured $CuCaAg_2Se$–graphene–TiO_2 ternary nanocomposite. New J. Chem. **44**, 16795–16809 (2020)
215. Z. Otgonbayar, Y. Liu, K.Y. Cho, C.-H. Jung, W.-C. Oh, Novel ternary composite of $LaYAgO_4$ and TiO_2 united with graphene and its complement: Photocatalytic performance of CO_2 reduction into methanol. Mater. Sci. Semicond. Process. **121**, 105456 (2021)
216. X. Chang, T. Wang, J. Gong, CO_2 photo-reduction: insights into CO_2 activation and reaction on surfaces of photocatalysts. Energy Environ. Sci. **9**, 2177–2196 (2016)
217. S. Xie, Q. Zhang, G. Liu, Y. Wang, Photocatalytic and photoelectrocatalytic reduction of CO_2 using heterogeneous catalysts with controlled nanostructures. Chem. Commun. **52**, 35–59 (2016)
218. C.-W. Huang, V.-H. Nguyen, S.-R. Zhou, S.-Y. Hsu, J.-X. Tan, K.C.-W. Wu, Metal–organic frameworks: preparation and applications in highly efficient heterogeneous photocatalysis. Sustain. Energy Fuels **4**, 504–521 (2020)
219. Q. Chen, S. Sun, Y. Wang, Q. Zhang, L. Zhu, Y. Liu, In-situ remediation of phosphogypsum in a cement-free pathway: utilization of ground granulated blast furnace slag and NaOH pretreatment. Chemosphere **313**, 137412 (2023)
220. Z. Zhang, Y. Zheng, L. Qian, D. Luo, H. Dou, G. Wen, A. Yu, Z. Chen, Emerging trends in sustainable CO_2-management materials. Adv. Mater. **34**, 2201547 (2022)
221. S. Wang, M. Xu, T. Peng, C. Zhang, T. Li, I. Hussain, J. Wang, B. Tan, Porous hypercrosslinked polymer-TiO_2-graphene composite photocatalysts for visible-light-driven CO_2 conversion. Nat. Commun. **10**, 676 (2019)
222. S. Wang, K. Song, C. Zhang, Y. Shu, T. Li, B. Tan, A novel metalporphyrin-based microporous organic polymer with high CO_2 uptake and efficient chemical conversion of CO_2 under ambient conditions. J. Mater. Chem. A **5**, 1509–1515 (2017)
223. K. Yuan, Y. Xu, J. Uihlein, G. Brunklaus, L. Shi, R. Heiderhoff, M. Que, M. Forster, T. Chassé, T. Pichler, Straightforward generation of pillared, microporous graphene frameworks for use in supercapacitors. Adv. Mater. **27**, 6714–6721 (2015)
224. S. Wang, C. Zhang, Y. Shu, S. Jiang, Q. Xia, L. Chen, S. Jin, I. Hussain, A.I. Cooper, B. Tan, Layered microporous polymers by solvent knitting method. Sci. Adv. **3**, e1602610 (2017)
225. Y. Liu, S. Wang, X. Meng, Y. Ye, X. Song, Z. Liang, Increasing the surface area and CO_2 uptake of conjugated microporous polymers via a post-knitting method. Mater. Chem. Frontiers **5**, 5319–5327 (2021)
226. Y. Sun, C. Liu, W. Su, Y. Zhou, L. Zhou, Principles of methane adsorption and natural gas storage. Adsorption **15**, 133–137 (2009)
227. Z. Xu, C. Zhuang, Z. Zou, J. Wang, X. Xu, T. Peng, Enhanced photocatalytic activity by the construction of a TiO_2/carbon nitride nanosheets heterostructure with high surface area via direct interfacial assembly. Nano Res. **10**, 2193–2209 (2017)
228. J. Wang, L. Huang, R. Yang, Z. Zhang, J. Wu, Y. Gao, Q. Wang, D. O'Hare, Z. Zhong, Recent advances in solid sorbents for CO_2 capture and new development trends. Energy Environ. Sci. **7**, 3478–3518 (2014)
229. L. Tan, B. Tan, Hypercrosslinked porous polymer materials: design, synthesis, and applications. Chem. Soc. Rev. **46**, 3322–3356 (2017)
230. X. Yang-Fan, Y. Mu-Zi, C. Bai-Xue, W. Xu-Dong, C. Hong-Yan, K. Dai-Bin, S. Cheng-Yong, A CsPbBr3 perovskite quantum dot/graphene oxide composite for photocatalytic CO_2 reduction (2017).
231. Z. Gu, B. Zhang, Y. Asakura, S. Tsukuda, H. Kato, M. Kakihana, S. Yin, Alkali-assisted hydrothermal preparation of g-C_3N_4/rGO nanocomposites with highly enhanced photocatalytic NO_x removal activity. Appl. Surf. Sci. **521**, 146213 (2020)
232. A. Kumar, K. Sharma, M. Thakur, D. Pathania, A. Sharma, Fabrication of high visible light active $LaFeO_3$/Cl-g-C_3N_4/RGO heterojunction for solar assisted photo-degradation of aceclofenac. J. Environ. Chem. Eng. **10**, 108098 (2022)
233. Z. Zhan, H. Wang, Q. Huang, S. Li, X. Yi, Q. Tang, J. Wang, B. Tan, Grafting hypercrosslinked polymers on TiO_2 surface for anchoring ultrafine Pd nanoparticles: dramatically enhanced efficiency and selectivity toward photocatalytic reduction of CO_2 to CH_4. Small **18**, 2105083 (2022)
234. G.E. Schukraft, R.T. Woodward, S. Kumar, M. Sachs, S. Eslava, C. Petit, Hypercrosslinked polymers as a photocatalytic platform for visible-light-driven CO_2 photoreduction using H_2O. Chemsuschem **14**, 1720–1727 (2021)
235. T. Garg, A. Goyal, A. Kaushik, S. Singhal, State-of-the-art evolution of g-C_3N_4 based Z-scheme heterostructures towards energy and environmental applications: a review. Mater. Res. Bull. **2023**, 11248 (2023)
236. M. Mirzaei, A.H. Rasouli, A. Saedi, HOMO–LUMO photosensitization analyses of coronene-cytosine complexes. Main Group Chem. **20**, 565–573 (2021)
237. K. Suenaga, A. Watanabe, K. Tanaka, Y. Chujo, Design for a pure-blue-emissive polymer film through the selective perturbation of the energy level of the highest occupied molecular orbital in a boron complex. Macromolecules **56**, 6419–6425 (2023)
238. Y. Chai, Y. Kong, M. Lin, W. Lin, J. Shen, J. Long, R. Yuan, W. Dai, X. Wang, Z. Zhang, Metal to non-metal sites of metallic sulfides switching products from CO to CH_4 for photocatalytic CO_2 reduction. Nat. Commun. **14**, 6168 (2023)

239. H. Hu, Y. He, H. Yu, D. Li, M. Sun, Y. Feng, C. Zhang, H. Chen, C. Deng, Constructing a noble-metal-free 0D/2D CdS/SnS2 heterojunction for efficient visible-light-driven photocatalytic pollutant degradation and hydrogen generation. Nanotechnology **34**, 505712 (2023)
240. F. Zhang, Y.-H. Li, M.-Y. Qi, Y.M. Yamada, M. Anpo, Z.-R. Tang, Y.-J. Xu, Photothermal catalytic CO_2 reduction over nanomaterials. Chem. Catal. **1**, 272–297 (2021)
241. P. Netzsch, F. Pielnhofer, H.A. Höppe, From S-O–S to B–O–S to B–O–B Bridges: Ba [B (S2O7) 2] 2 as a model system for the structural diversity in borosulfate chemistry. Inorg. Chem. **59**, 15180–15188 (2020)
242. H. Chen, J. Xu, H. Lin, Z. Wang, Z. Liu, Multi-cycle aqueous arsenic removal by novel magnetic n/s-doped hydrochars activated via one-pot and two-stage schemes. Chem. Eng. J. **429**, 132071 (2022)
243. X. Xiong, C. Mao, Z. Yang, Q. Zhang, G.I. Waterhouse, L. Gu, T. Zhang, Photocatalytic CO_2 reduction to CO over Ni single atoms supported on defect-rich zirconia. Adv. Energy Mater. **10**, 2002928 (2020)
244. L. Zhang, X. Yang, F. Zhang, G. Long, T. Zhang, K. Leng, Y. Zhang, Y. Huang, Y. Ma, M. Zhang, Controlling the effective surface area and pore size distribution of sp2 carbon materials and their impact on the capacitance performance of these materials. J. Am. Chem. Soc. **135**, 5921–5929 (2013)
245. D. Sundar, C.-H. Liu, S. Anandan, J.J. Wu, Photocatalytic CO_2 conversion into solar fuels using carbon-based materials—a review. Molecules **28**, 5383 (2023)
246. S. Peng, J. Gao, D. Stojkov, S. Yousefi, H.U. Simon, Established and emerging roles for mitochondria in neutrophils. Immunol. Rev. **314**, 413–426 (2023)
247. M. Yang, P. Wang, Y. Li, S. Tang, X. Lin, H. Zhang, Z. Zhu, F. Chen, Graphene aerogel-based NiAl-LDH/g-C_3N_4 with ultratight sheet-sheet heterojunction for excellent visible-light photocatalytic activity of CO_2 reduction. Appl. Catal. B **306**, 121065 (2022)
248. S. Gong, M. Hou, Y. Niu, X. Teng, X. Liu, M. Xu, C. Xu, V.K.-M. Au, Z. Chen, Molybdenum phosphide coupled with highly dispersed nickel confined in porous carbon nanofibers for enhanced photocatalytic CO_2 reduction. Chem. Eng. J. **427**, 131717 (2022)
249. X.-Q. Zhang, W.-C. Li, A.-H. Lu, Designed porous carbon materials for efficient CO_2 adsorption and separation. New Carbon Mater. **30**, 481–501 (2015)
250. X.-Q. Zhang, W.-C. Li, A.-H. Lu, Designed porous carbon materials for efficient CO_2 adsorption and separation. Carbon **100**, 260 (2016)
251. P. Zhang, Y. Dong, Z. Ren, G. Wang, Y. Guo, C. Wang, Z. Ma, Rapid urbanization and meteorological changes are reshaping the urban vegetation pattern in urban core area: a national 315-city study in China. Sci. Total. Environ. **904**, 167269 (2023)
252. U. Kamran, S.-J. Park, Chemically modified carbonaceous adsorbents for enhanced CO_2 capture: a review. J. Clean. Prod. **290**, 125776 (2021)
253. M. Zhang, C. Lai, B. Li, F. Xu, D. Huang, S. Liu, L. Qin, X. Liu, H. Yi, Y. Fu, Insightful understanding of charge carrier transfer in 2D/2D heterojunction photocatalyst: Ni–Co layered double hydroxides deposited on ornamental g-C_3N_4 ultrathin nanosheet with boosted molecular oxygen activation. Chem. Eng. J. **422**, 130120 (2021)
254. K. Fan, Z. Jin, H. Yang, D. Liu, H. Hu, Y. Bi, Promotion of the excited electron transfer over Ni-and Co-sulfide co-doped g-C3N4 photocatalyst (g-C3N4/NixCo1− xS2) for hydrogen production under visible light irradiation. Sci. Rep. **7**, 7710 (2017)
255. J. Lian, W. Liu, L. Meng, J. Wu, A. Zeb, L. Cheng, Y. Lian, H. Sun, Effects of microplastics derived from polymer-coated fertilizer on maize growth, rhizosphere, and soil properties. J. Clean. Prod. **318**, 128571 (2021)
256. Y. Li, Z. He, L. Liu, Y. Jiang, W.-J. Ong, Y. Duan, W. Ho, F. Dong, Inside-and-out modification of graphitic carbon nitride (g-C3N4) photocatalysts via defect engineering for energy and environmental science. Nano Energy **105**, 108032 (2023)
257. J. Wang, Y. Song, C. Zuo, R. Li, Y. Zhou, Y. Zhang, B. Wu, Few-layer porous carbon nitride anchoring Co and Ni with charge transfer mechanism for photocatalytic CO_2 reduction. J. Colloid Interface Sci. **625**, 722–733 (2022)
258. V.S. Vyas, V.W.-H. Lau, B.V. Lotsch, Soft photocatalysis: organic polymers for solar fuel production. Chem. Mater. **28**, 5191–5204 (2016)
259. T. Banerjee, F. Podjaski, J. Kröger, B.P. Biswal, B.V. Lotsch, Polymer photocatalysts for solar-to-chemical energy conversion. Nat. Rev. Mater. **6**, 168–190 (2021)
260. J. Hou, T. Jiang, X. Wang, G. Zhang, J.-J. Zou, C. Cao, Variable dimensional structure and interface design of g-C3N4/BiOI composites with oxygen vacancy for improving visible-light photocatalytic properties. J. Clean. Prod. **287**, 125072 (2021)
261. H. An, B. Lin, C. Xue, X. Yan, Y. Dai, J. Wei, G. Yang, Formation of BiOI/g-C_3N_4 nanosheet composites with high visible-light-driven photocatalytic activity. Chin. J. Catal. **39**, 654–663 (2018)
262. J. Liang, X. Li, J. Zuo, J. Lin, Z. Liu, Hybrid 0D/2D heterostructures: in-situ growth of 0D g-C 3 N 4 on 2D BiOI for efficient photocatalyst. Adv. Compos. Hybrid Mater. **4**, 1122–1136 (2021)
263. W. Shen, Y. Lu, J.A. Hu, H. Le, W. Yu, W. Xu, W. Yu, J. Zheng, Mechanism of miR-320 in regulating biological characteristics of ischemic cerebral neuron by mediating Nox_2/ROS pathway. J. Mol. Neurosci. **70**, 449–457 (2020)
264. Z. You, C. Wu, Q. Shen, Y. Yu, H. Chen, Y. Su, H. Wang, C. Wu, F. Zhang, H. Yang, A novel efficient gC_3N_4@ BiOI p–n heterojunction photocatalyst constructed through the assembly of gC_3N_4 nanoparticles. Dalton Trans. **47**, 7353–7361 (2018)
265. F. Kuttassery, H. Kumagai, R. Kamata, Y. Ebato, M. Higashi, H. Suzuki, R. Abe, O. Ishitani, Supramolecular photocatalysts fixed on the inside of the polypyrrole layer in dye sensitized molecular photocathodes: application to photocatalytic CO_2 reduction coupled with water oxidation. Chem. Sci. **12**, 13216–13232 (2021)
266. D.H. Apaydin, E. Tordin, E. Portenkirchner, G. Aufischer, S. Schlager, M. Weichselbaumer, K. Oppelt, N.S. Sariciftci, Photoelectrochemical reduction of CO_2 using third-generation conjugated polymers. ChemistrySelect **1**, 1156–1162 (2016)
267. Z. Wang, X.-F. Zhang, L. Shu, J. Yao, Copper sulfide integrated functional cellulose hydrogel for efficient solar water purification. Carbohydr. Polym. **319**, 121161 (2023)
268. M.A. Rosen, Environmental sustainability tools in the biofuel industry. Biofuel Res. J. **5**, 751–752 (2018)
269. M. Aghbashlo, Z. Khounani, H. Hosseinzadeh-Bandbafha, V.K. Gupta, H. Amiri, S.S. Lam, T. Morosuk, M. Tabatabaei, Exergoenvironmental analysis of bioenergy systems: a comprehensive review. Renew. Sustain. Energy Rev. **149**, 111399 (2021)
270. M. Aghbashlo, H. Hosseinzadeh-Bandbafha, H. Shahbeik, M. Tabatabaei, The role of sustainability assessment tools in realizing bioenergy and bioproduct systems. Biofuel Res. J. **9**, 1697–1706 (2022)